SAN-1285-T2

THIN FILMS OF SILICON ON METALLURGICAL SILICON SUBSTRATES

Final Report for September 1, 1976—September 30, 1979

By
Ting L. Chu

September 1979

Work Performed Under Contract No. EY-76-C-03-1285

Southern Methodist University
Dallas, Texas

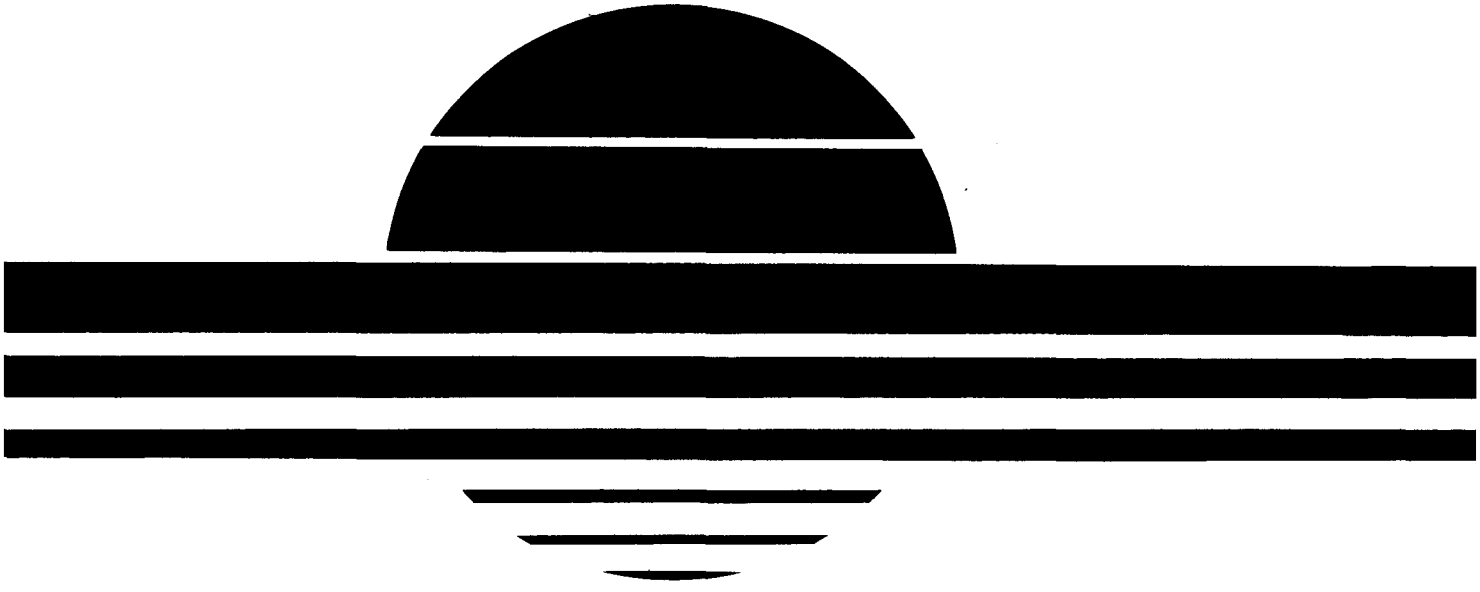

U.S. Department of Energy

Solar Energy

DISCLAIMER

Available from the National Technical Information Service, U. S. Department of Commerce, Springfield, Virginia 22161.

Price: Paper Copy $8.00
Microfiche $3.50

SAN-1285-T2
Distribution Category UC-63c

THIN FILMS OF SILICON ON METALLURGICAL SILICON SUBSTRATES

Final Report

Covering the Period September 1, 1976 to September 30, 1979

Prepared under DOE Contract DE-AC03-76-ET-20405

by

Ting L. Chu, Principal Investigator

Southern Methodist University

Dallas, Texas 75275

September, 1979

CONTENTS

List of Illustrations

List of Tables

Summary

This is the Final Report of a research program "Thin Films of Silicon on Metallurgical Silicon Substrates" sponsored by the U. S. Department of Energy under Contract No. EY-76-C-03-1285. The objectives of this program are to investigate thin films of silicon on metallurgical silicon substrates and to demonstrate an AM1 efficiency of 10% for thin film silicon solar cells.

The principal approach used in this work is the deposition of a silicon film of controlled thickness and dopant distribution on a purified metallurgical silicon substrate. Efforts have been directed to (1) the purification of metallurgical silicon, (2) the preparation of metallurgical silicon substrates, (3) the deposition and characterization of silicon films on metallurgical silicon substrates, (4) the properties of polycrystalline silicon p-n junctions on metallurgical silicon substrates, (5) the fabrication and characterization of silicon solar cells on purified metallurgical silicon substrates, (6) the investigation of stability of thin film polycrystalline silicon solar cells, and (7) the reduction of the electrical effects of grain boundaries.

During the course of this program, a number of significant results have been obtained. Metallurgical silicon has been purified by a low cost technique, acid-extraction and phosphorus pentoxide treatment, to yield materials suitable for substrate purposes. Recrystallization techniques have been developed to produce large grain silicon sheet supported on graphite. Silicon films of controlled thickness and dopant distribution have been deposited on metallurgical silicon substrates, and the properties of silicon films and epitaxial p-n junctions have been investigated in detail. Many polycrystalline silicon solar cells have been fabricated, and their properties including current-voltage characteristics, spectral response, minority carrier diffusion length, dopant profile, and stability, have been characterized in detail. The properties of grain boundaries in polycrystalline silicon solar cells have been investigated by photoresponse scan and EBIC techniques. The conversion efficiency of polycrystalline silicon solar cells can be increased significantly by heat treatment; however, no definitive conclusions on the mechanism of heat treatment have been established. At present, the best solar cells of 9 cm^2 area have an AM1 efficiency of about 9.75%.

I. Introduction

This is the Final Report of a research program "Thin Films of Silicon on Metallurgical Silicon Substrates" supported by the Division of Solar Technology of the U. S. Department of Energy under Contract No. EY-76-C-03-1285. The objectives of this contract are to perform intensive studies concerning thin films of silicon on metallurgical silicon substrates and to demonstrate an AM1 efficiency of 10% for thin film silicon solar cells.

The principal approach used in this work is the deposition of a silicon film of controlled thickness and dopant concentration on a purified metallurgical silicon substrate by the thermal reduction of trichlorosilane, the most economical process for the manufacture of polycrystalline silicon. Metallurgical silicon was selected as the substrate because of its crystal structure and low cost. Although extensive investigations on the use of low-cost foreign substrates, such as aluminum,[1] steel,[2] graphite,[3] ceramic,[4] etc. have been carried out, the silicon film always consisted of relatively small crystallites, 25 μm or less, and the solar cells have low conversion efficiencies because of the recombination of light-generated carriers at grain boundaries. Since silicon is an indirect gap material with a very gradual absorption edge, relative long minority carrier diffusion length, 25 μm or longer, is required for reasonable collection efficiencies, and crystallite size should be many times larger than the diffusion length in order that the carrier loss at grain boundaries is insignificant.

During the course of this program, major efforts were directed to (1) the purification of metallurgical silicon, (2) the preparation of metallurgical silicon substrates, (3) the deposition and characterization of silicon films on metallurgical silicon substrates, (4) the properties of polycrystalline silicon p-n junctions on metallurgical silicon substrates, (5) the fabrication and characterization of silicon solar cells on purified metallurgical silicon substrates, (6) the reduction of the electrical effects of grain boundaries, and (7) the investigation of the stability and reliability of thin film polycrystalline silicon solar cells. Solar cells of 9 cm^2 area with AM1 efficiencies of up to 9.8% have been prepared. The experimental procedures and results are discussed in the following sections.

II. Purification of Metallurgical Silicon

The principal approach to the fabrication of solar cells developed in this program is the deposition of the active region on a purified metallurgical silicon substrate. The development of low cost techniques to reduce impurity contents in metallurgical silicon to a tolerable level is an important factor determining the eventual success of this approach.

Metallurgical silicon is manufactured by the reduction of sand with carbonaceous reducing agents in a submerged electric arc furnace at 1700°-1900°C, and the resulting silicon melt is discharged into molds for solidification. It is of about 98% purity and contains iron and aluminum at concentrations of a few tenths of one percent and other metallic impurities (such as boron, chromium, copper, nickel, titanium, zinc, etc.) at concentrations of up to several hundred parts per million. The impurity content in metallurgical silicon is excessive for device purposes. The current process used in semiconductor industry for the purification of metallurgical silicon consists of (1) the conversion of metallurgical silicon into trichlorosilane by reaction with hydrogen chloride, (2) the purification of trichlorosilane, and (3) the reduction of trichlorosilane with hydrogen. This sequence of processing is tedious, and step (3) is extremely energy-intensive increasing the cost of silicon by about seventy times. Because of this high cost of purification via the halide intermediate, several direct purification techniques have been attempted during the fifties. They include:

(A) The treatment of molten silicon with gaseous chemical reagents to selectively remove specific impurities from the melt.[5] It has been

claimed that molten silicon could be purified by treatment with a mixture of halogen (or a halogen derivative) and oxygen, and that 3 kg of technical grade silicon (98%) was purified to 99.99% purity in only 3 min. by the reaction with an equi-molecular mixture of oxygen and hydrogen chloride.

(B) The treatment of pulverized metallurgical-grade silicon with aqua regia, sulfuric acid, hydrofluoric acid, etc., producing silicon suitable for microwave diodes.[6]

(C) The remelting of silicon under a layer of fused silicate which getters various impurities.[7] For example, chemical analysis has shown that after three hours of treatment, the concentrations of iron and aluminum were reduced from 4.5% and 1.80% to 1.20% and 0.83%, respectively.

The chemical treatment of the melt and the acid-extraction of pulverized material have been investigated for the purification of metallurgical silicon. The experimental procedures and results are discussed in the following sections.

II. 1 Chemical Treatment of Melt

Thermodynamic data indicated that the treatment of molten metallurgical silicon with chlorine or hydrogen chloride is effective in reducing the concentration of impurities, such as aluminum and titanium, which are chemically more reactive than silicon. However, impurities less reactive than silicon, such as copper and iron, cannot be readily removed in this manner. Since most metallic impurities in silicon have low segregation coefficients, unidirectional solidification is an effective technique for the removal of these impurities from metallurgical silicon. Thus, the

unidirectional solidification technique was incorporated into the chemical treatment technique for the purification of metallurgical silicon.

II. 1. 1 Experimental

The apparatus used for the purification of metallurgical silicon by a combination of chemical treatment and unidirectional solidification is shown schematically in Fig. 1. It consisted of a fused silica tube of 69 mm ID containing a silica crucible in a graphite susceptor, and gas inlet tubes were provided to flow argon through the fused silica tube and to introduce the gaseous reagent into the melt. To carry out the purification process, metallurgical silicon was placed in the fused silica crucible, and with argon flowing through the silica tube, the graphite susceptor was heated externally with an rf generator. After the silicon became molten, the gaseous reagent was bubbled through the melt until about 10% of the silicon had been reacted and volatilized. The graphite susceptor was then slowly lowered, and the solidification took place from the bottom of the charge in the upward direction. The resulting material was cut into wafers perpendicular to the direction of solidification, and wafers from four different positions (bottom, 1/3 from the bottom, 2/3 from the bottom, and the top) were used for analysis. Each wafer was dissolved in a nitric acid-hydrofluric acid mixture, neutralized with ammonium hydroxide, and the resulting solution was analyzed for aluminum and iron by the atomic absorption technique.

To further evaluate the usefulness of chemical treatment plus unidirectional solidification for the purification of metallurgical silicon, single crystals of about 2.5 cm diameter were pulled from chlorine-treated, chlorine and oxygen treated, and chlorine-treated plus

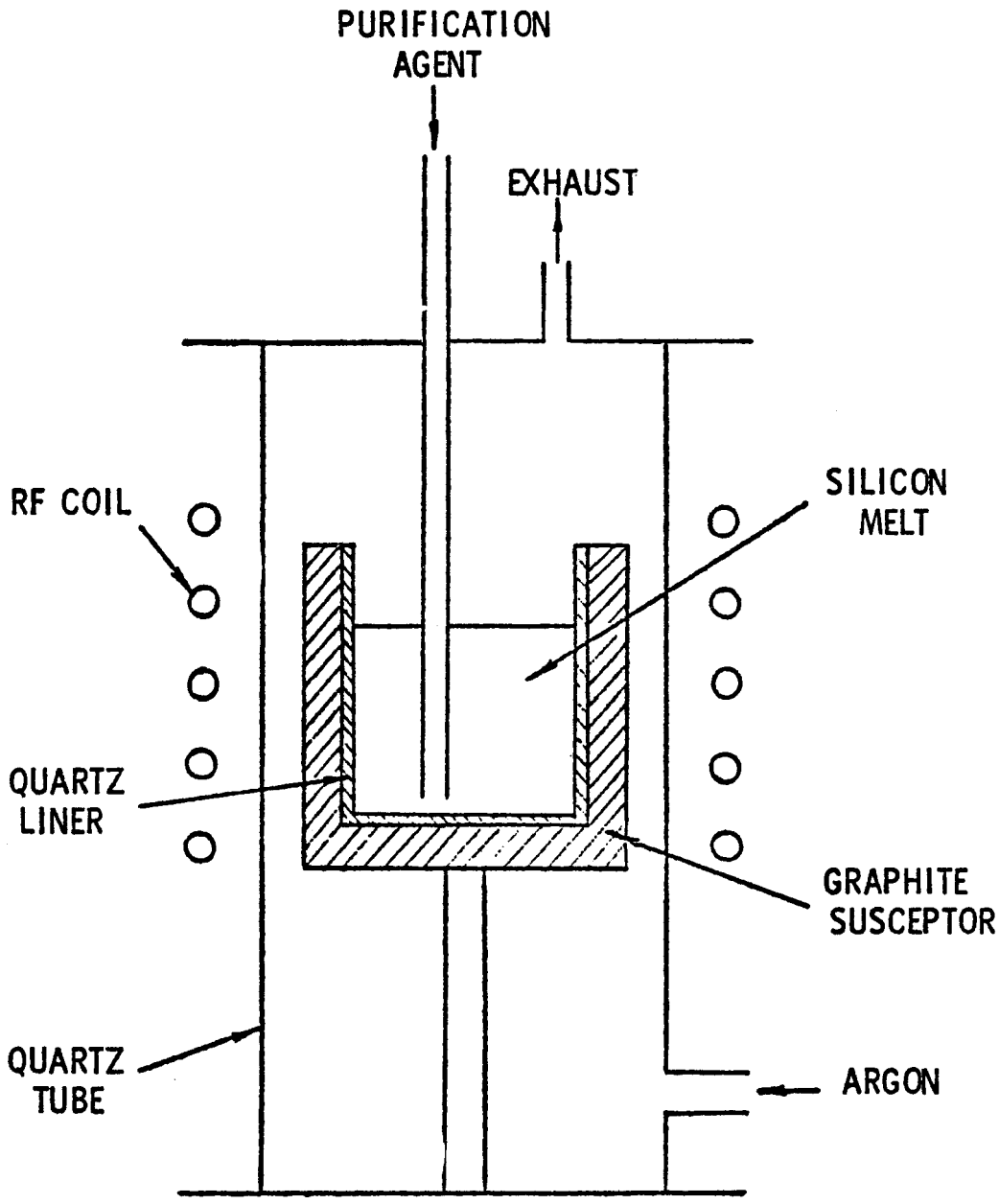

Figure 1 Schematic diagram of the apparatus for the purification of metallurgical silicon.

unidirectional solidified metallurgical silicon. The Czochralski crystal pulling was carried out in a helium atmosphere at a rate of about 10 cm/hr, and 75% to 90% of the charge was pulled. The crystal was sawed, and the wafers, after etching with a nitric acid-hydrofluoric acid mixture, were used for resistivity and Hall measurements in the temperature range of 81-350°K. Ohmic contacts to the specimens were made by evaporating titanium-silver to the surface through a metal mask followed by annealing in a hydrogen atmosphere at 550°C.

II. 1.2. Results

The results of analysis of chlorine-treated plus unidirectionally solidified metallurgical silicon are shown in Table I; it is noted that the concentrations of aluminum and iron in the bottom half of the charge have been reduced substantially. The emission analysis of two sections of a chlorine-treated plus unidirectionally solidified sample is shown in Table II, together with the impurity content in metallurgical silicon.

The upper sections of all three crystals are p-type with room temperature resistivities of approximately 0.32, 0.26, and 0.14 ohm-cm for chlorine-treated, chlorine and oxygen-treated, and chlorine-treated plus unidirectional solidified material, respectively. Their Hall mobility-temperature relations in the temperature range 81°-305°K are shown in Figure 2. In this temperature range, the crystal from chlorine-treated plus unidirectionally solidified metallurgical silicon has higher mobilities than the others. However, the room temperature mobilities in all crystals (81, 108 and 127 cm^2/V-sec for chlorine-treated, chlorine and oxygen-treated, and chlorine-treated unidirectionally solidified materials, respectively)

Table I Concentration of impurities (ppm by weight) in metallurgical silicon purified by chlorine treatment and unidirectional solidification determined by atomic absorption

Element	Bottom	1/3 from the bottom	2/3 from the bottom	Top
Fe	<10	<10	680	27,800
Al	<100	<100	<100	<100

Table II Concentration of impurities (ppm by weight) in metallurgical silicon purified by chlorine treatment and unidirectional solidification determined by emission analysis

Element	Metallurgical Silicon	Purified Material Bottom Section	Purified Material 2/3 from bottom
Al	>>1000	<10	<10
B	10 - 100	N.D.	N.D.
Ca	---	<10	<10
Cr	30 - 300	N.D.	10 - 100
Cu	10 - 100	<10	<10
Fe	>>1000	<10	10 - 100
Mg	10 - 100	<10	<10
Mn	30 - 300	N.D.	<10
Ni	10 - 100	N.D.	N.D.
Pb	---	<10	<10
Ti	30 - 300	N.D.	<10
V	100 - 1000	N.D.	10 - 100
Ag	---	<10	10 - 100

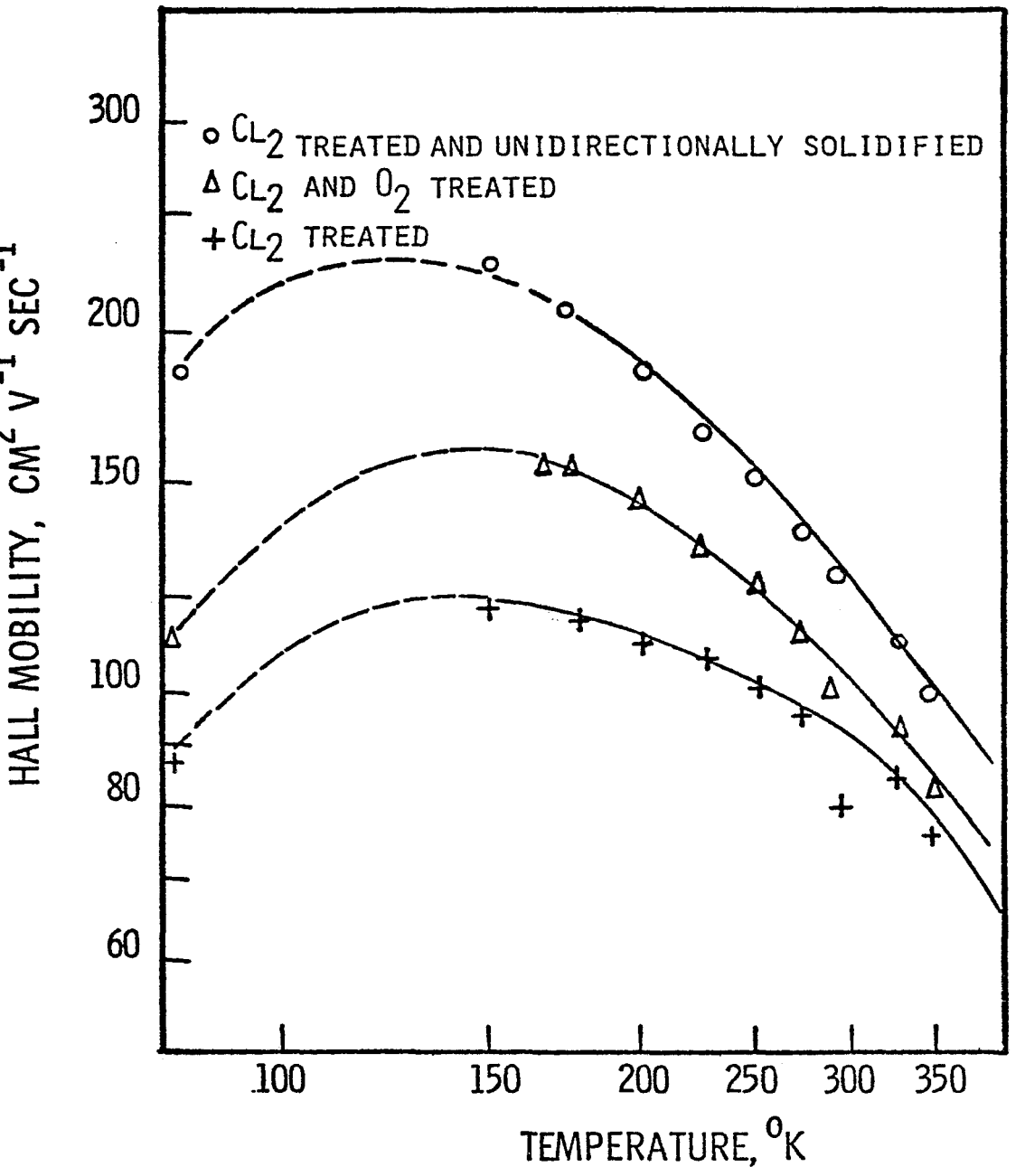

Fig. 2. Hall mobilities of holes in the upper section of silicon crystals pulled from metallurgical silicon purified by chlorine treatment, chlorine and oxygen treatment, and chlorine treatment plus unidirectional solidification.

are significantly lower than those in semiconductor grade silicon of similar carrier concentrations (higher than 200 cm^2/V-sec). Furthermore, the mobility-temperature relations peak at temperatures considerably higher than those observed in semiconductor grade silicon of similar carrier concentrations. These results indicate compensation in crystals pulled from purified metallurgical silicon. Although the incorporation of unidirectional solidification into chemical treatment provides a more efficient way for the purification of metallurgical silicon than chemical treatment alone, the resulting silicon still has a relatively high concentration of residual impurities.

Figure 3 shows the plots of $\sigma/\mu_H q$ versus the reciprocal of absolute temperature for all three crystals, where $\sigma/\mu_H q$ is directly proportional to the net carrier concentration. These relations are linear with a slope of $-E_I/2k$, where E_I is the ionization energy of the dopant. The ionization energy deduced in this manner is 0.044-0.052 eV, suggesting boron as the acceptor impurity. Furthermore, the relatively slow change in Hall mobility with temperature (μ_H in the chlorine-treated plus unidirectionally solidified material varies approximately with T^{-1} in the temperature range 150° to 350°K) indicates that the donors have similar ionization energies as the acceptor.

The minority carrier diffusion length in silicon slices from chlorine treated plus unidirectionally solidified material, measured by the steady-state surface photovoltage method at room temperature (cf. Section VI), was found to be 25 $\pm$ 2 μm. As a comparison, silicon slices from chlorine treated and chlorine-oxygen treated metallurgical silicon had diffusion lengths of (4-5) $\pm$ 1 μm, again indicating the effectiveness of unidirectional

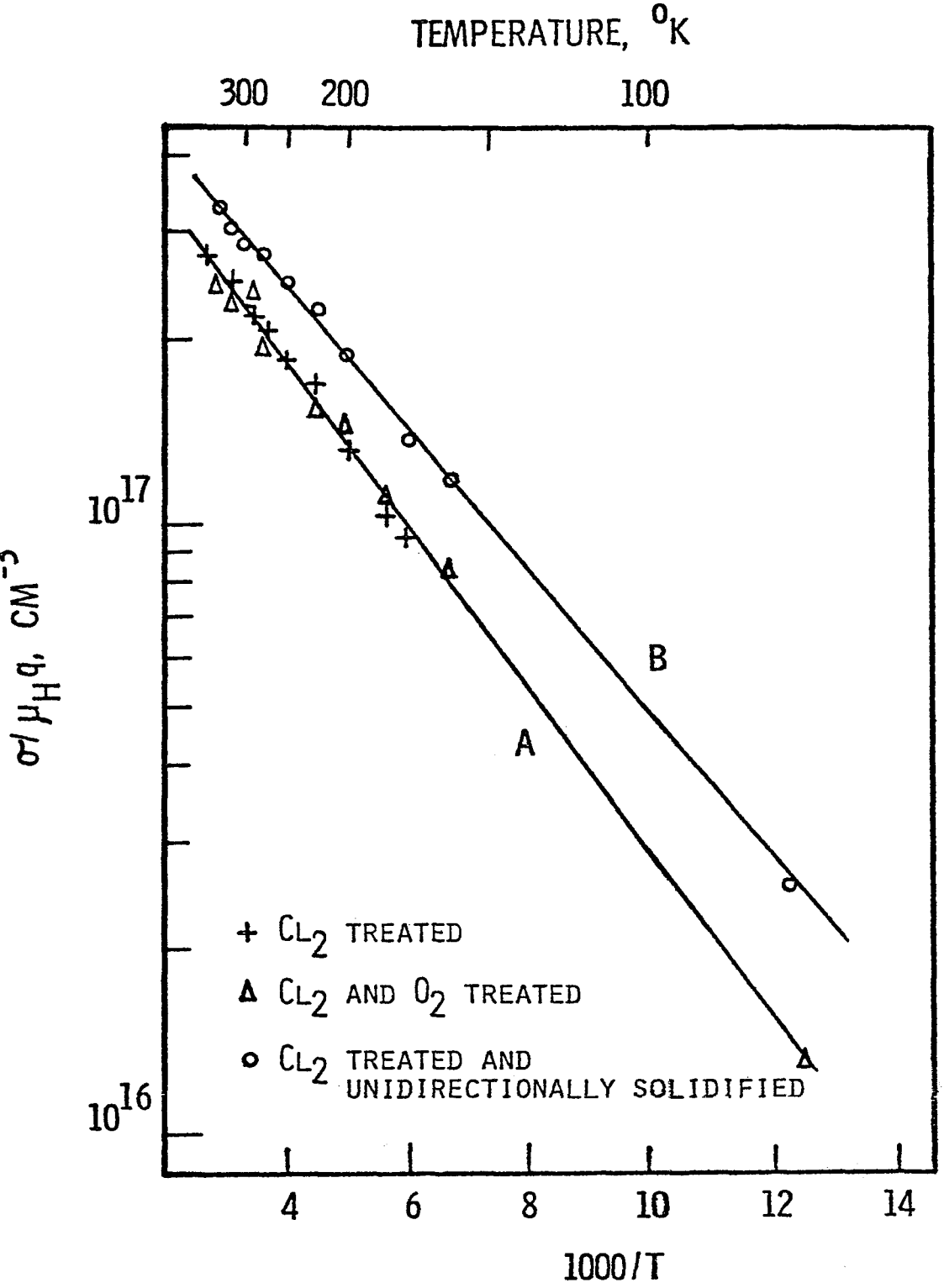

Fig. 3. Relations between $\sigma/\mu_H q$ and reciprocal temperature for the upper section of silicon crystals pulled from metallurgical silicon purified by chlorine treatment, chlorine-oxygen treatment, and chlorine treatment plus unidirectional solidification.

solidification.

II. 2 Acid Extraction

The chemical treatment of molten metallurgical silicon and the subsequent unidirectional solidification of the melt have been shown to be effective in reducing substantially the concentrations of aluminum and iron in metallurgical silicon. However, this process is energy-intensive and not sufficiently economical for large scale operations, and lower-temperature purification techniques, such as the acid-extraction technique, were investigated.

Although many metallic impurities such as iron, aluminum, copper, gold, nickel, titanium, etc., are highly soluble in molten silicon, their solubilities in solid silicon are relatively low. For example, the solubilities of iron, copper, and aluminum in silicon at 850°C are approximately 2×10^{15}, 7×10^{16}, and 10^{19} cm^{-3}, respectively, and are lower at lower temperatures. [8] Thus, during the solidification of molten metallurgical silicon in the manufacturing process, a major portion of the low-solubility impurities should precipitate at grain boundaries or at interstitial position. When the cast metallurgical silicon blocks are pulverized, the breakage occurs mostly at grain boundaries. The small grains, 1 mm for example, are either single crystalline or are aggregates of several single crystals. Therefore, a major portion of the metallic impurities are concentrated at the surface of the grains, and the treatment of pulverized metallurgical silicon with acids should be effective in removing these impurities as well as the impurities at grain boundaries. In addition to the work of Voos, [6] it has been claimed that over 90% of all impurities except boron, copper, and phosphorus can be removed

from metallurgical silicon in this manner.[9]

II. 2. 1 Experimental Procedure and Results

The effectiveness of the acid-extraction technique depends on the particle size of metallurgical silicon, the chemical reactivity of the acid, and the temperature and duration of treatment. A series of acid extraction experiments have been carried out using hydrochloric acid, aqua regia, and an equivolume mixture of sulfuric acid and nitric acid. Metallurgical silicon of 30-80 mesh in size with an iron content of 0.35%, purchased from the Ferroalloys Division of the Union Carbide Corporation, was used directly without further treatment. Usually 1.5 kg of silicon was heated with 1.5 liters of the acid under reflux conditions in a 3 liter flask for 4-5 days, and the acid was replaced 3-4 times. The concentration of iron in each acid extract and in the resulting silicon was determined by a spectrophotometric method described below.

Ferrous ion forms colored complexes with a number of organic reagents in aqueous solutions. These complexes exhibit distinct absorption bands in the visible region with high absorption coefficients, and the concentration of iron in a solution can be determined from its absorbance at the peak of the absorption band. The use of 1,10-phenanthroline, $C_{12}N_2H_8$, as a complex agent has been used for the quantitative determination of iron in fruit juices and biological materials.[10, 11] Ferric ions can be reduced to the ferrous state by using hydroxylamine hydrochloride. The complex formed, an octahedrally coordinated ferrous ion and three molecules of 1,10-phenanthroline, has an absorption band peaking at about 510 nm. At low concentrations, the intensity of this peak is directly proportional to the concentration of the iron in solution when

an excess of the complex agent is present. For example, an aqueous solution with an iron concentration of 0.10 ppm at a thickness of 1 cm shows a transmittance of 95.5% at 510 nm. Thus this technique is suitable for the quantitative determination of iron at very low concentrations. To determine the concentration of iron in silicon, a weighed quantity of the specimen is dissolved in an ammonium fluoride-nitric acid mixture (20 g NH_4F in 100 ml 70% HNO_3); ammonium fluoride was used instead of hydrofluoric acid because of the presence of a relatively high concentration of iron in hydrofluoric acid, about 17 μg/mℓ. Thus, the system is complicated by the presence of high concentrations of silicon, fluoride, and nitrate ions. After the dissolution of the silicon sample, the solution is neutralized with ammonia to a P_H of 2-2.5. Subsequently, 5 mℓ of an aqueous solution of hydroxylamine hydrochloride (10% by weight) is added to reduce the ferric ions to the ferrous state, and 15 mℓ of an aqueous solution of 1,10-phenathroline (0.3% by weight) is added to form the complex (this amount is four times the stoichiometric amount required to complex all the iron in a 5 ppm solution). However, no color develops until the P_H of the solution is increased to 6.5; a white precipitate, presumably silicic acid, forms at higher P_H values. It has been found that the P_H of the solution is the most important factor determining the reliability and reproducibility of this spectrophotometric technique. The solution is then diluted to a known volume, and its absorbance is measured at 510 nm. To determine the accuracy of this procedure described above, a series of solutions containing 0.5 to 5 ppm of iron were prepared by dissolving semiconductor grade silicon in an ammonium fluoride-nitric acid solution followed by the addition of a

known amount of a standard iron solution. The optical absorbance of these solutions at 510 nm was then measured, and a good linear relation is observed between absorbance and the concentration of iron in solution.

The first acid extract always contained the highest concentration of iron, and the iron concentration decreased rapidly with further extractions. For example, the iron concentrations in the first, second, and third aqua regia extracts contain 151, 22.5, and 5.8 μg of iron per cubic centimeter, respectively. Hydrochloric acid has been found to be the least effective for the removal of iron, and iron concentration in hydrochloric acid-treated silicon is 850-900 ppma. Aqua regia and the sulfuric acid-nitric acid mixture are considerably more effective than hydrochloric acid. The iron concentration in aqua regia-treated silicon is 600-650 ppma.

II. 2. 2 Further Improvements by Phosphorus Pentoxide Treatment

The acid-extraction technique is based on the assumptions that the major portion of metallic impurities precipitates at grain boundaries during the solidification of metallurgical silicon and that the pulverization of metallurgical silicon takes place at grain boundaries. The fact that acid treated metallurgical silicon still contains an appreciable concentration of iron indicates that metallic impurities also precipitate within the grains. In an attempt to remove these impurities, acid-treated metallurgical silicon was heated in a hydrogen atmosphere at 1000-1050°C for 4 hours and slowly cooled with the objective that the metallic impurities would diffuse to the surface or grain boundaries. However, the extraction of heat-treated material with aqua regia did not appreciably reduce the iron content in silicon. This could be due to the slowness of the dissolution of, or the relatively low solubility of, metallic impurities at the

annealing temperature used.

The precipitation of metallic impurities in silicon has been extensively investigated, [12, 13] and gettering with phosphorus or boron oxide can be used to remove these metallic impurities.[14, 15] It has been established that during gettering with phosphorus pentoxide, the concentration of metallic impurities in the n^+ surface region is considerably higher than that in the oxide glass.[16, 17] The gettering technique was investigated for the purification of metallurgical silicon. About 200 g of aqua regia-treated metallurgical silicon was mixed with 10 g of phosphorus pentoxide and a small amount of water to form a thick paste. This mixture was dried and heated in air at 1050°C for 4 days. The resulting mass was treated with diluted hydrofluoric acid to remove the phosphosilicate glass and refluxed with aqua regia for several days. The iron content in silicon analyzed by the spectrophotometric technique is about 250 ppma, as compared with 650 ppma in the starting material. A relatively high concentration of phosphorus is introduced into metallurgical silicon during the gettering process. The gettered metallurgical silicon yields 0.03 ohm-cm n-type material after recrystallization and is suitable as a substrate for the deposition of p^+/n solar cells.

III. Preparation and Characterization of Metallurgical Silicon Substrates

The preparation of metallurgical silicon substrates is a most important processing step in the fabrication of thin film polycrystalline silicon solar cells. When a metallurgical silicon substrate is used for the deposition of the active region of the solar cell, the chemical and structural defects in the substrate greatly affect the characteristics of the solar cell. A unidirectional solidification technique and a zone-melting technique have been used in this program to yield metallurgical silicon sheets on graphite plates with relatively large crystallites.

III. 1 Unidirectional Solidification Technique

In this technique, the entire charge of silicon supported on a graphite plate is melted, and the solidification of the melt is controlled to take place from one end of the specimen to the other. A schematic diagram of the apparatus is shown in Fig. 4. Partially purified metallurgical silicon was placed on a graphite plate, 15 cm long and 5 cm wide, in a fused silica tube of 65 mm ID, and the graphite was heated externally by an rf generator. The spacings between the turns of the rf coil were adjusted to yield a unidirectional temperature gradient of 50°-80°C along the length of the specimen. The entire specimen was first heated at a temperature above the melting point of silicon, and the input power was reduced for the solidification to take place from one end of the specimen to the other. This unidirectional solidification is essential because of the higher density of liquid silicon. The regions which solidify last become grossly polycrystalline with a protruded surface due

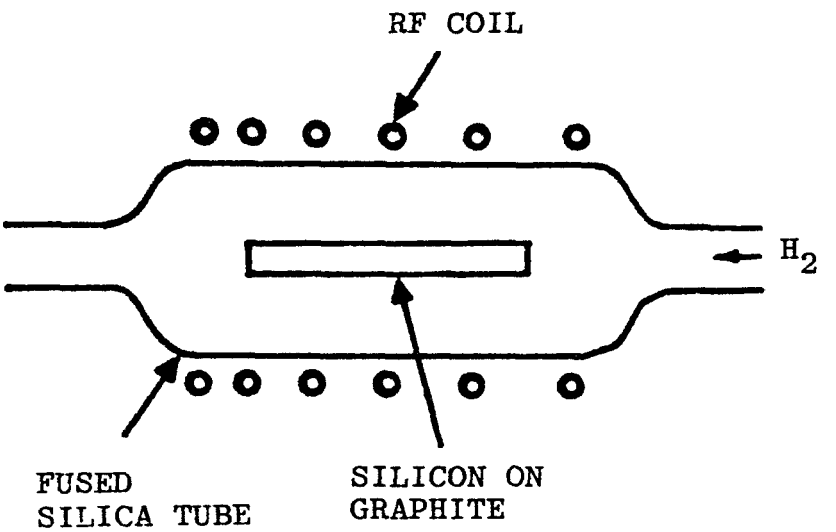

Figure 4 A schematic diagram of the apparatus for the preparation of silicon substrate by unidirectional solidification.

to the expansion of silicon on solidification. Also, the solidification process should initiate from the surface of the melt and proceed inward to minimize the effects of random nucleations at the silicon-graphite interface.

The rate of solidification is determined by the rate of reduction of input power, the temperature gradient along the length of the specimen, and the flow rate of hydrogen. The crystallite size is determined by the rate of solidification, the shape of the solid-liquid interface, etc. Since the sides of the specimen are at lower temperatures than the center region due to heat losses, nucleation and growth take place along both the length and width directions of the specimen, and the size of crystallites are limited. The temperature gradient across the width of the specimen may be minimized by using radiation shields, thus promoting the nucleation and growth along the length direction.

The rate of solidification has been found to be the most important parameter affecting the morphology of the unidirectionally solidified material. At high rates of solidification, 3-5 cm/min, the surface is not planar with many ridges, faces, and valleys. Figures 5 and 6 show, respectively, the optical and scanning electron micrographs of such a surface, illustrating its unique appearance. The crystallites are elongated, up to 10 cm in length and several millimeters in width. All ridges are extremely straight, suggesting that they are the intersections of twin planes with the grown surface. When a specimen is cross-sectioned vertically perpendicular to a ridge and the cross sectioned surface

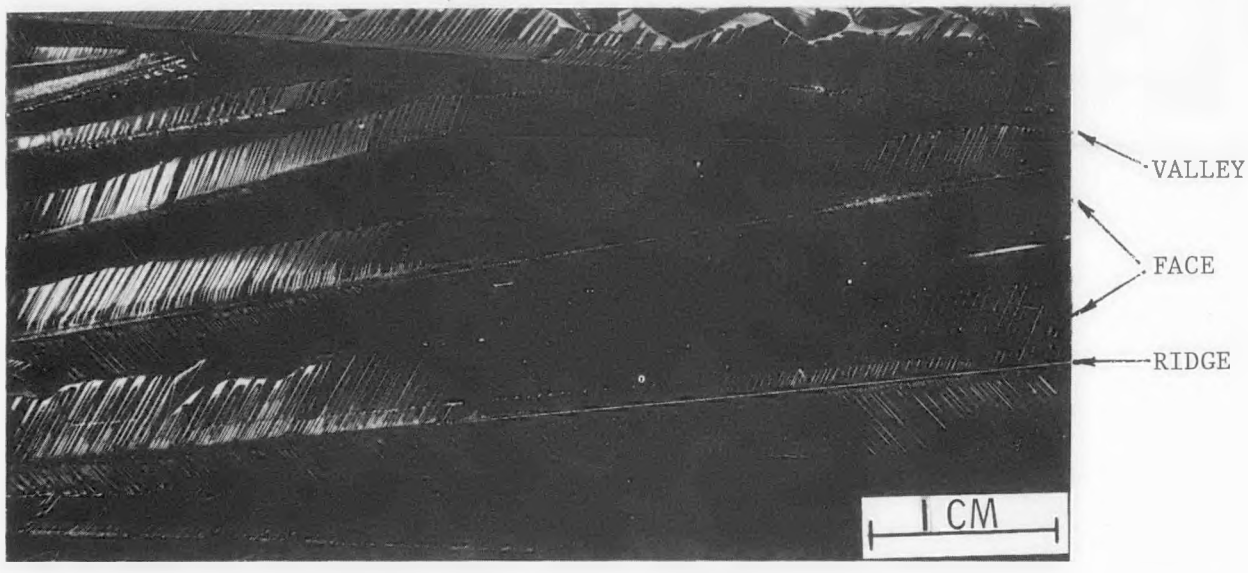

Figure 5 Optical photograph of the non-planar surface of a metallurgical silicon substrate showing ridges, faces, and valleys.

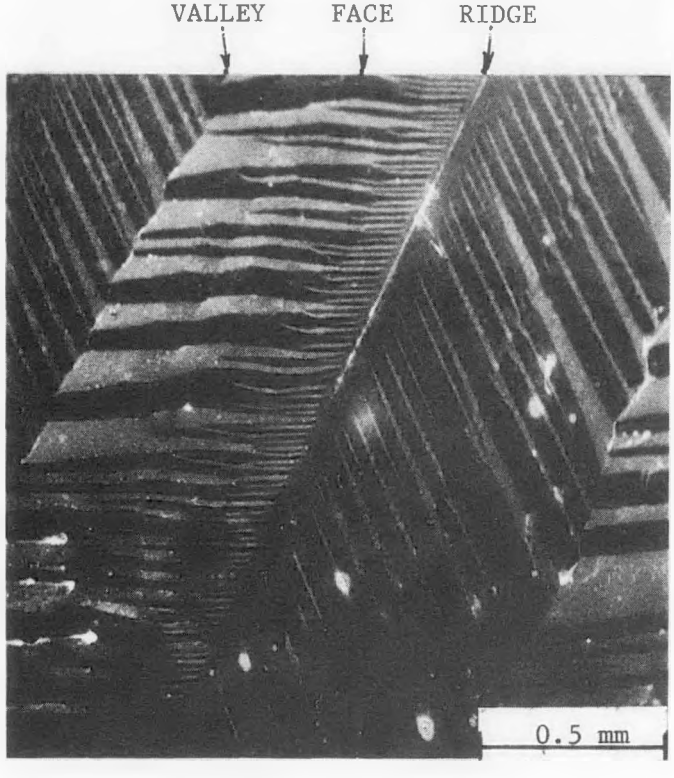

Figure 6 Scanning electron micrograph of the non-planar surface of a metallurgical silicon substrate showing ridges, faces, and valleys.

mechanically polished and chemically etched, etch traces of twin planes are revealed, as shown in Fig. 7. Most valleys are curved and are high angle grain boundaries. The X-ray diffraction technique was used to determine the crystallographic orientations of the faces of crystallites. The commonly observed orientations are {331},{531}, and high index planes from the twinning of {331} and {531} planes about a $\{\bar{1}11\}$ plane. The twinning of the (331) and (531) planes about the $(\bar{1}11)$ plane yields (11 7 1) and $(\bar{13}, \bar{11}, 5)$ planes, respectively. The angle between (331) and (11 7 1) is 164.8°, and that between (531) and $(\bar{13}\ \bar{11}\ 5)$ is 172.4°. In many cases, the measured angle between the two faces adjacent to a ridge is about 165°. Chemical etching has also revealed that the crystallites are usually multiple-twinned and the dislocation density varies widely from face to face.

At low rates of solidification, 0.5-1 cm/min, the surface of the resulting substrate is planar. This type of substrate also consists of elongated crystallites up to several centimeters in length. Chemical etching has revealed twin planes, grain boundaries, and dislocation clusters as the most common defects. Figure 8 shows the etched surface of an area with relatively high defect density, where the etch traces of twins and grain boundaries are apparent. X-ray diffraction examinations indicate that some areas show a very strong {110} preferred orientation while others a very strong {331} preferred orientation.

All metallurgical silicon substrates are n-type with an electrical resistivity of 0.02-0.03 ohm-cm. Spreading resistance measurements indicate that the resistivity is relatively uniform along the length of the specimen, 15 cm. To determine the iron distribution in the substrate

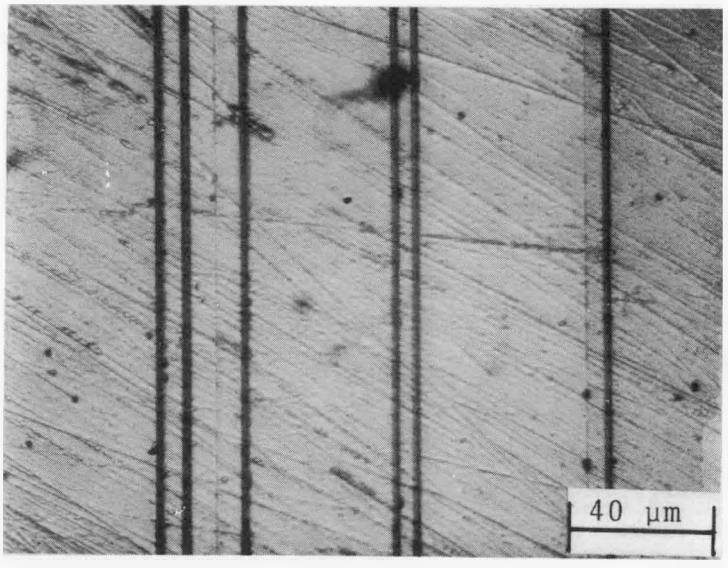

Figure 7 Polished and etched surface of the vertical cross section of a metallurgical silicon substrate with a non-planar surface cut perpendicular to a ridge.

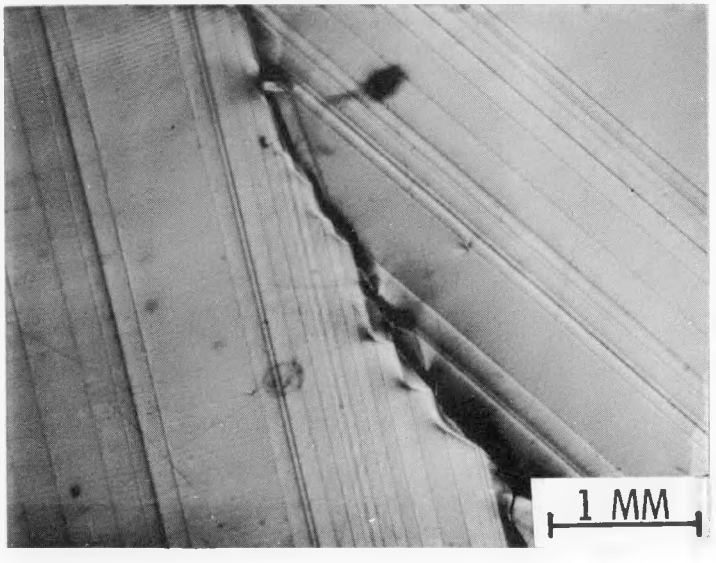

Figure 8 Etched surface of a planar metallurgical silicon substrate showing grain and twin boundaries.

along the direction of solidification, the substrate was cut into twelve pieces of about equal length, and the concentration of iron in silicon on each piece was determined. Substrates with planar and non-planar surfaces were analyzed. Although considerable segregation of iron is expected in slowly solidified material, the segregation was found to be negligible in both cases. The concentration of iron varied less than a factor of three along the length of the specimen. This is due probably to the high diffusion coefficient of iron in silicon at high temperatures, and the segregated impurities diffuse back into the solidified material.

III. 2. Zone-Melting

The stationary unidirectional solidification technique is not suitable for the preparation of large area substrates because of the excessive power required to maintain the entire silicon charge in the molten state over an extended time period. The preparation of metallurgical silicon substrate by the zone-melting technique was therefore investigated using the apparatus shown schematically in Fig. 9. Partially purified metallurgical silicon was placed on a graphite plate, 15 cm long and 5 cm wide, in a fused silicon tube of 65 mm ID, and the graphite was heated by an rf generator in a hydrogen flow. The turns of a small section of the rf coil is closely spaced to form a molten silicon zone of 1-2" width at one end of the specimen while the remainder was heated at 1000-1200^{o}C. The silicon/graphite specimen was then pulled to allow the molten zone to traverse through its length. At a pulling rate of 0.5-1 cm/min, planar surface similar to that of the unidirectionally solidified material prepared at similar rates was

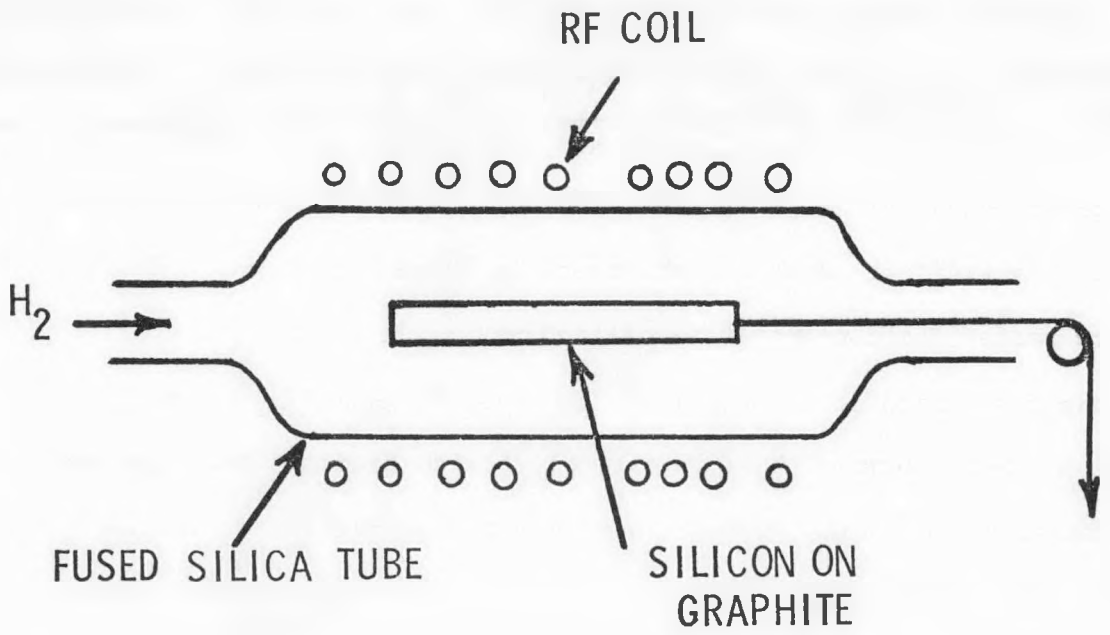

Figure 9 A schematic diagram of the apparatus for the preparation of metallurgical silicon substrates by zone-melting.

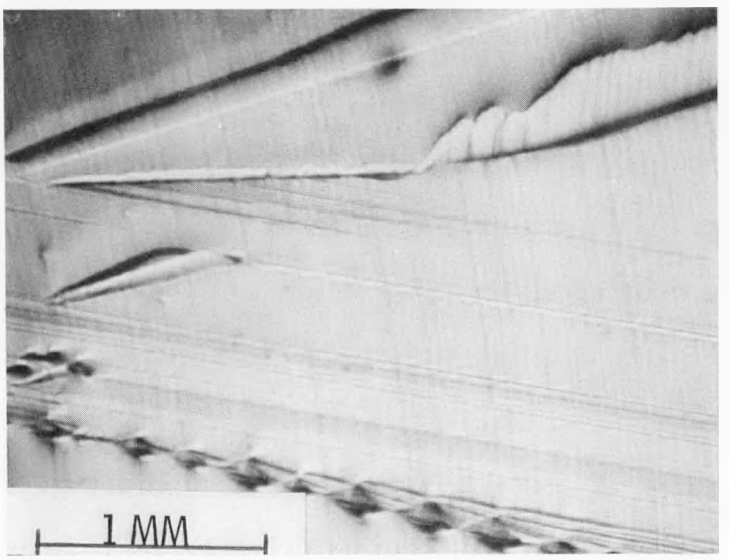

Figure 10 Chemically etched surface of zone-melted metallurgical silicon substrate.

obtained; however, growth steps are frequently observed because of the unevenness of pulling and the vibration of melt. This operation can be improved by using a moving rf coil instead of pulling the silicon/graphite assembly. Figure 10 shows the chemically etched surface of a zone-melted metallurgical silicon substrate, where traces of grain boundaries, twin boundaries, and growth steps are revealed.

IV. Deposition and Characterization of Silicon Films

IV. 1 The Deposition Process

Using partially purified metallurgical silicon recrystallized on graphite as subtrates, silicon films of controlled thickness, conductivity type, and dopant profile have been deposited at 1100°-1150°C by the thermal reduction of trichlorosilane containing appropriate dopants; the apparatus is shown schematically in Fig. 11. The trichlorosilane process is widely used in the manufacture of semiconductor grade polycrystalline silicon and is most cost-effective for the deposition of silicon films.

The apparatus consists of two parts: the gas flow control and the reaction tube. The flow of various gases is directed by appropriate valves and measured by flowmeters. Trichlorosilane is kept in a double-wall stainless steel cylinder provided with gas inlet and outlet tubes, and a constant temperature fluid is circulated through the jacket of the container to maintain the temperature of trichlorosilane at 8°C. Trichlorosilane is introduced into the reaction tube by bubbling hydrogen through the liquid. Hydrogen is purified by diffusion through a palladium silver alloy. By varying the flow rate of hydrogen through trichlorosilane, deposition rates in the range of 0.2 μm/min-2 μm/min can be readily obtained. Using diborane and phosphine of appropriate concentrations in hydrogen and proper dilution systems when necessary, p-type and n-type silicon films with resistivities in the range of 0.003-1 ohm-cm can be deposited. The reaction tube is a fused silica tube of 65 mm ID, and the metallurgical silicon/graphite substrate is placed in the reaction tube and heated externally with an rf generator.

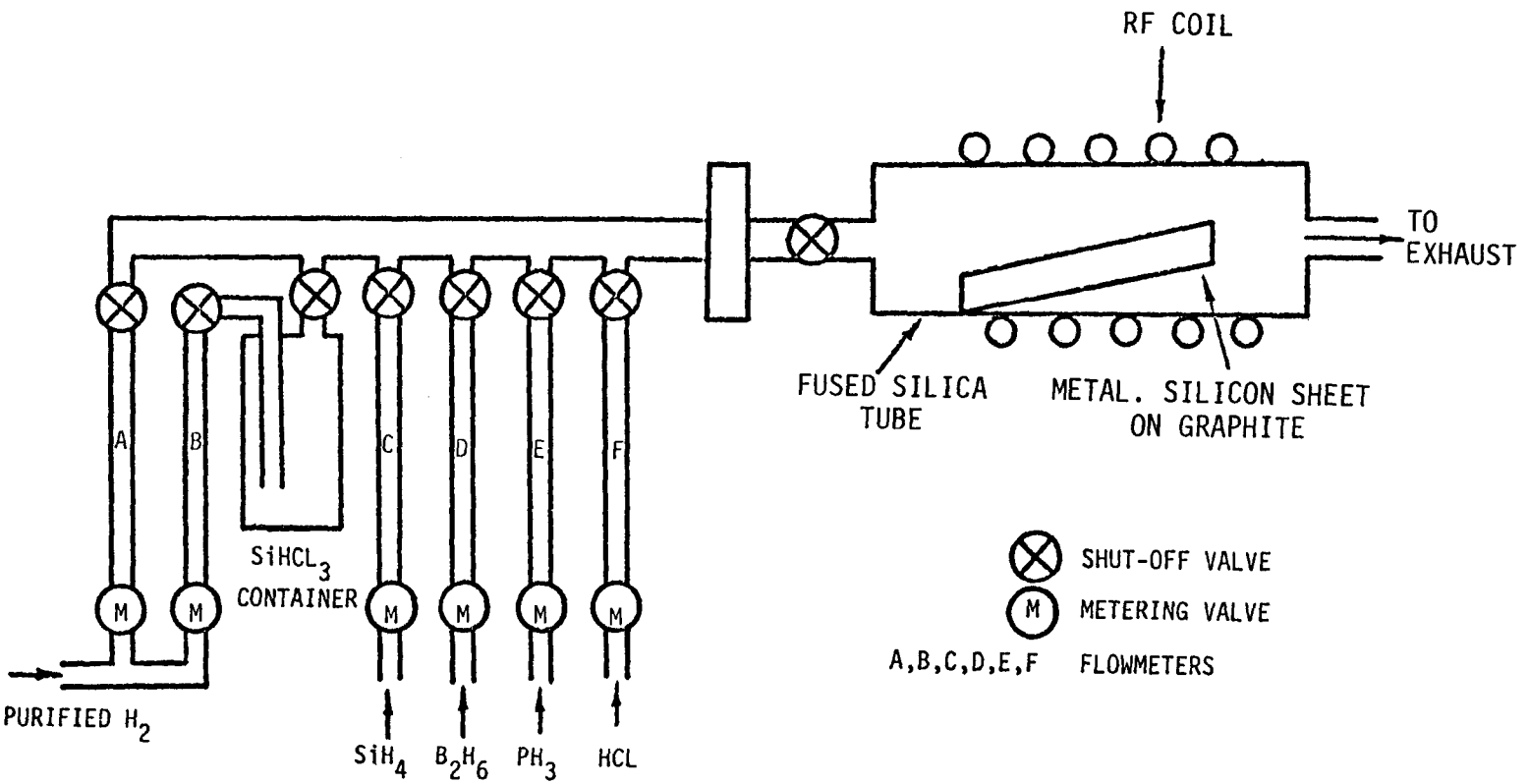

Figure 11. Schematic diagram of the apparatus for the chemical vapor deposition of silicon films.

Prior to the deposition process, the substrate was heated in hydrogen at about 1250°C for 20 min to remove any oxide on the surface; in-situ etching with hydrogen chloride was not used when the deposition of silicon was carried out immediately after the substrate preparation. A high flow rate of hydrogen, 20 ℓ/min, was used to insure uniformity in both thickness and resistivity of the deposited film. In all cases, the deposited silicon was found to be epitaxial with respect to the substrate by metallographic examinations.

IV. 2 Chemical Impurities in Silicon Films

Since iron is the major impurity in metallurgical silicon and iron diffuses rapidly at temperatures used for the deposition of silicon films, the concentration profile of iron in the thickness direction of the film was determined. A specimen with a silicon film of about 25 μm thickness on metallurgical silicon substrates was used. The silicon film was dissolved at about 2 μm intervals, and the iron concentration in each solution was found to be essentially the same, similar to the iron concentration in the substrate, about 200 ppma. Thus, iron has diffused from the substrate through the silicon film during the deposition process.

The results of chemical analysis indicate that the concentration of iron in silicon films far exceeds the solubility of iron in silicon at room temperature. Thus, the silicon films become supersaturated with iron, and the excess iron should precipitate. By forming a shallow p-n junction in the silicon film during the deposition process and examining the resulting film with a scanning electron microscope in the electron beam induced current (EBIC) mode, the presence of impurity precipitates

has been observed. Figure 12 shows the EBIC micrograph of one region of a shallow p-n junction structure on a metallurgical silicon substrate. All grain boundaries are clearly delineated because of the reduced collection of beam-induced current. In addition, there are numerous small dots in the grains showing varying degrees of low collection efficiency. These dots are most likely impurity precipitates since they redistribute after heat treatment. Figure 13 shows the EBIC micrograph of the same region as shown in Fig. 12 after heat treatment at 950°C for 0.5 hr, where a noticeable fraction of the impurity precipitates has diffused to structural defects such as grain boundaries. In addition, iron silicide has been detected at grain boundaries by the ESCA technique[18].

IV. 3 Hall Mobility and Potential Barriers in Silicon Films

Since metallurgical silicon substrates are of n-type conductivity, p-type silicon films were deposited for ease of characterization. The Hall mobilities in several silicon films were measured at room temperature by the van der Pauw technique. The specimens were about 1 cm x 1 cm in area and contained one or more grain boundaries. Four contacts were made to the silicon layer along the circumference of the specimen by evaporating titanium and silver through a metal mask followed by annealing in hydrogen at 525°C. Current was passed between two alternating contacts, and the change in potential between the other two contacts due to the magnetic field was measured. The resistivity, Hall mobility, and carrier concentrations were then calculated from the Hall voltage. Reproducible results were obtained only in specimens with carrier concentrations higher than about 10^{17} cm^{-3}, and the measured

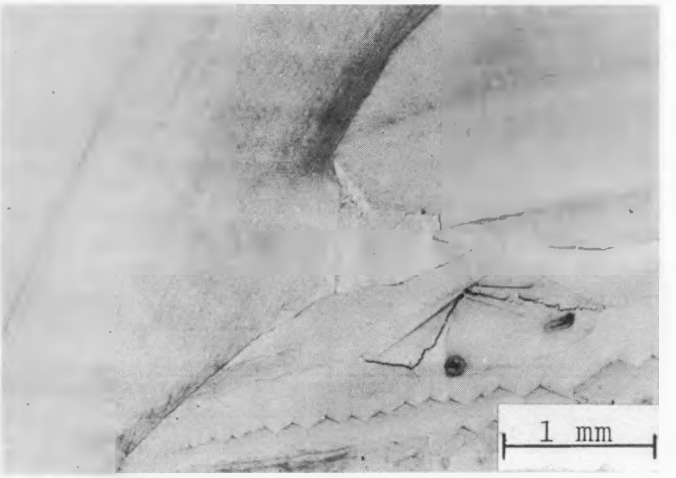

Figure 12 EBIC micrograph of one region of a shallow p-n junction structure on a metallurgical silicon substrate showing impurity precipitates.

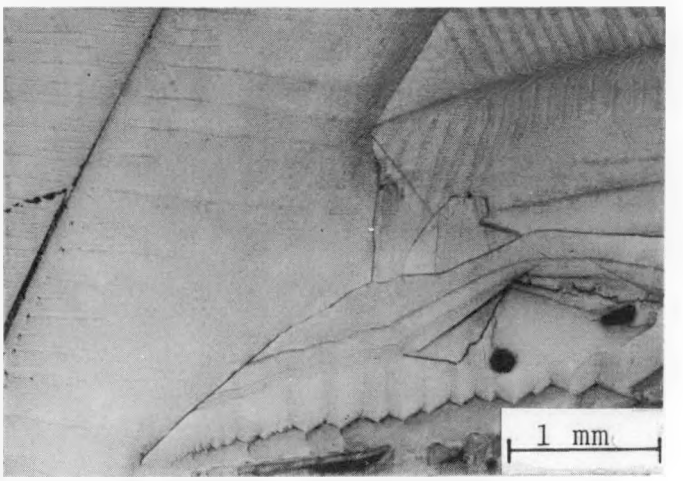

Figure 13 EBIC micrograph of the same region in Figure 12 after heat treatment at 950°C for 0.5 hr.

mobilities were slightly lower than those in single crystalline silicon of similar carrier concentrations. At lower carrier concentrations, however, the results were erratic and irreproducible due to the potential barriers at grain boundaries.

The potential barriers at grain boundaries in silicon films were investigated by using a high resolution potential probe apparatus. The p/n+ specimens were cut into strips of about 0.3 cm width and 1.5 cm length, and the cutting was carried out in such a manner that twin and grain boundaries were approximately parallel to the width of the specimen. Current contacts were then applied to both ends of the long dimension by evaporating titanium and silver through a metal mask followed by annealing, and lead wires were attached to the contacts by using conducting epoxy. The specimen was mounted on the mechanical stage of a toolmaker's microscope, where its position can be controlled with an accuracy of 0.01 mm by two micrometers. Since the direction of the current flow was approximately perpendicular to twin and grain boundaries, the potential variation along the current path was measured by using a fixed contact (one current contact) and a moving probe. The moving probe had a radius of curvature of 2.5×10^{-3} cm at its tip and was supported in such a manner that it could be readily placed on the surface of the specimen with a known fixed force without dragging. A measurable voltage drop was observed at all grain boundaries; the magnitude of the voltage drop increases rapidly with the resistivity of the silicon film and becomes appreciable in materials of 0.2 ohm-cm resistivity or higher. Figure 14 shows the potential gradient in a

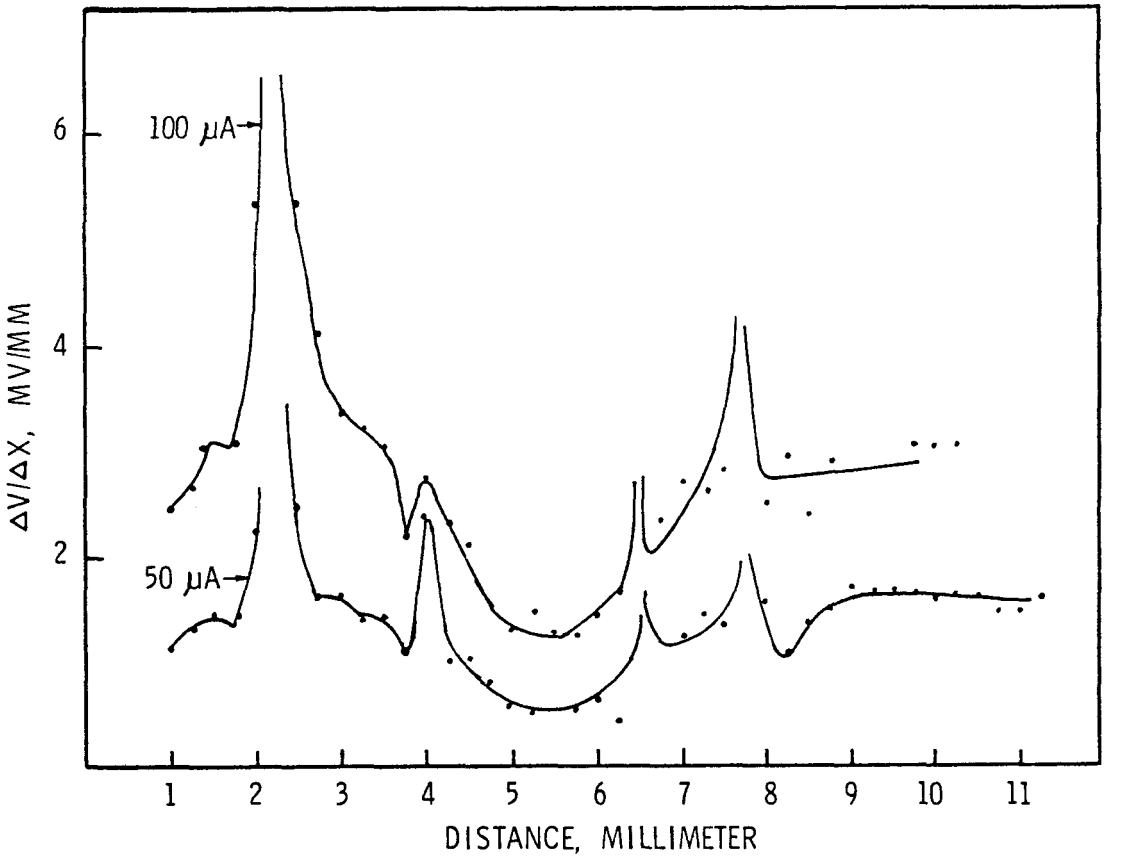

Fig. 14 Potential gradient as a function of probe position in a p-type silicon film of 1 ohm-cm resistivity on a metallurgical silicon substrate.

p-type film of 1 ohm-cm resistivity, where the measurements were carried out at 25 μm intervals and at two current levels, 100 μA and 50 μA. The change in potential gradient at grain boundaries are very pronounced; however, the potential drop is not directly proportional to current and also depends on the direction of current flow.

V. Polycrystalline Silicon P-N Junctions

Since the p-n junction in a solar cell is forward biased during its operation, the dark current-voltage characteristics of a solar cell is an important factor affecting its conversion efficiency. Excessive junction current degrades the power output of the solar cell by reducing the fill factor and the open-circuit voltage. To better understand the effects of grain boundaries on the characteristics of solar cells, a number of mesa diodes have been fabricated on various regions of an epitaxial p-n junction deposited on purified and unidirectionally solidified metallurgical silicon substrates. Their dark characteristics were measured over a wide temperature range, analyzed on the basis of the two-exponential model, and compared with those of epitaxial mesa diodes on single crystalline silicon substrates.

V. 1. Preparation of Epitaxial Mesa Diodes

Epitaxial structures of the configuration 10 μm n^+-silicon/ 25 μm p-type silicon/p^+-metallurgical silicon (partially purified and recrystallized)/ graphite were prepared in the usual manner. Ohmic contact was formed on the n^+-surface by evaporating successively titanium and silver followed by annealing at 525°C in hydrogen for 15 min., and mesa diodes were made at regions of the specimen with high angle grain boundaries and regions without grain boundaries (single crystal or twinned crystal) by masking and etching techniques. The area of each mesa diode was measured by using a plainmeter on an enlarged photograph. The junction surface was passivated by using about 1 μm of silicon dioxide deposited by the thermal oxidation of silane at 400°C. Subsequently, the silicon dioxide in the center region of each mesa was removed by masking and etching, and the two wires for

current and voltage leads were soldered to the exposed metal contact. A schematic diagram of the configuration of a mesa diode is shown in Fig. 15. The silicon dioxide passivation, a relatively thick n^+-layer, and a direct contact to the p^+-layer were used to reduce the shunting current and to minimize the series resistance.

V. 2. Current-Voltage Characteristics

The current-voltage characteristics of the diodes were measured by mounting the specimen in a vacuum tight brass chamber filled with dry nitrogen, and fourteen glass-metal feed throughs were used to provide current and voltage connections from six diodes and the p^+-region to the measurement equipment. The entire chamber was placed in a constant temperature bath containing silicon oil. The current-voltage measurements were carried out between the n^+-contact of each diode and the p^+-region by the four-probe technique at four temperatures in the range of 1° to 90°C. The voltage across the diode and the current through the diode were measured. Five measurements were made for each decade of current. At any given current, the voltage was usually reproducible within $\pm$ 0.3 mV.

The characteristics of more than eighty mesa diodes with the p-region of 0.1-1 ohm-cm resistivity have been measured. Emphasis has been directed to the comparison of forward characteristics of diodes deposited on regions with and without grain boundaries. Figure 16 shows the current-voltage characteristics of one diode with a grain boundary and one diode without grain boundaries at 274°, 297°, 324.5°, and 358°K. These diodes were of approximately 0.05 cm^2 in area, and the resistivity of the p-region was 0.1 ohm-cm. At a given voltage, the diode with a grain boundary invariably shows higher current density than that without a grain boundary.

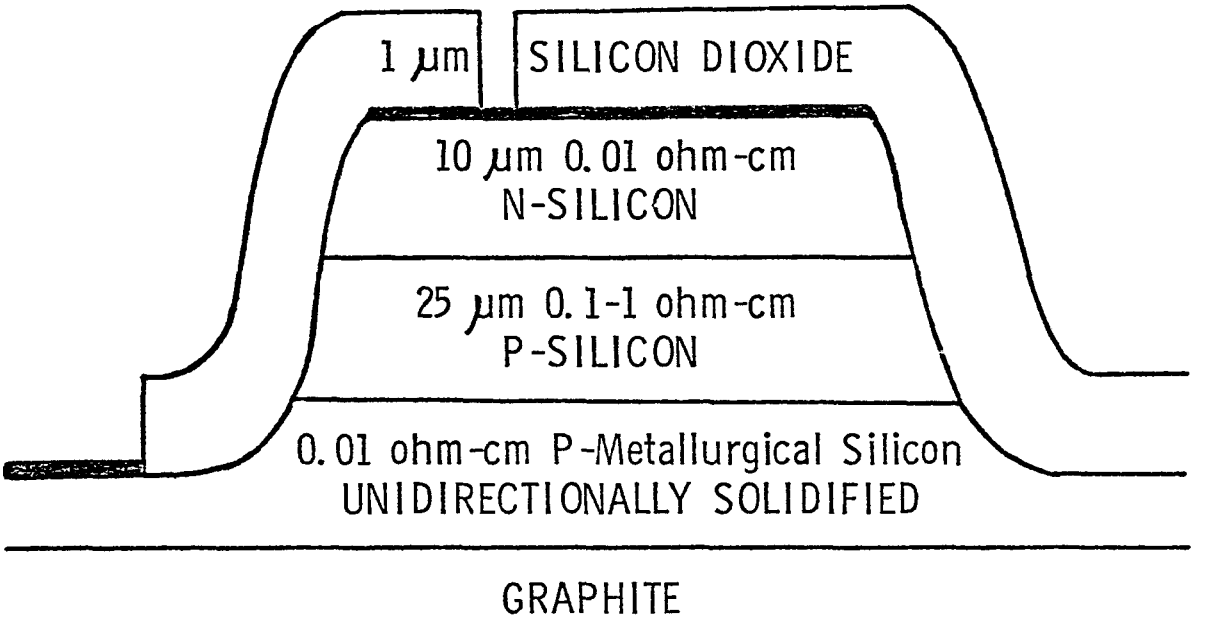

Fig.15 The configuration of a passivated epitaxial silicon mesa diode for current-voltage measurements.

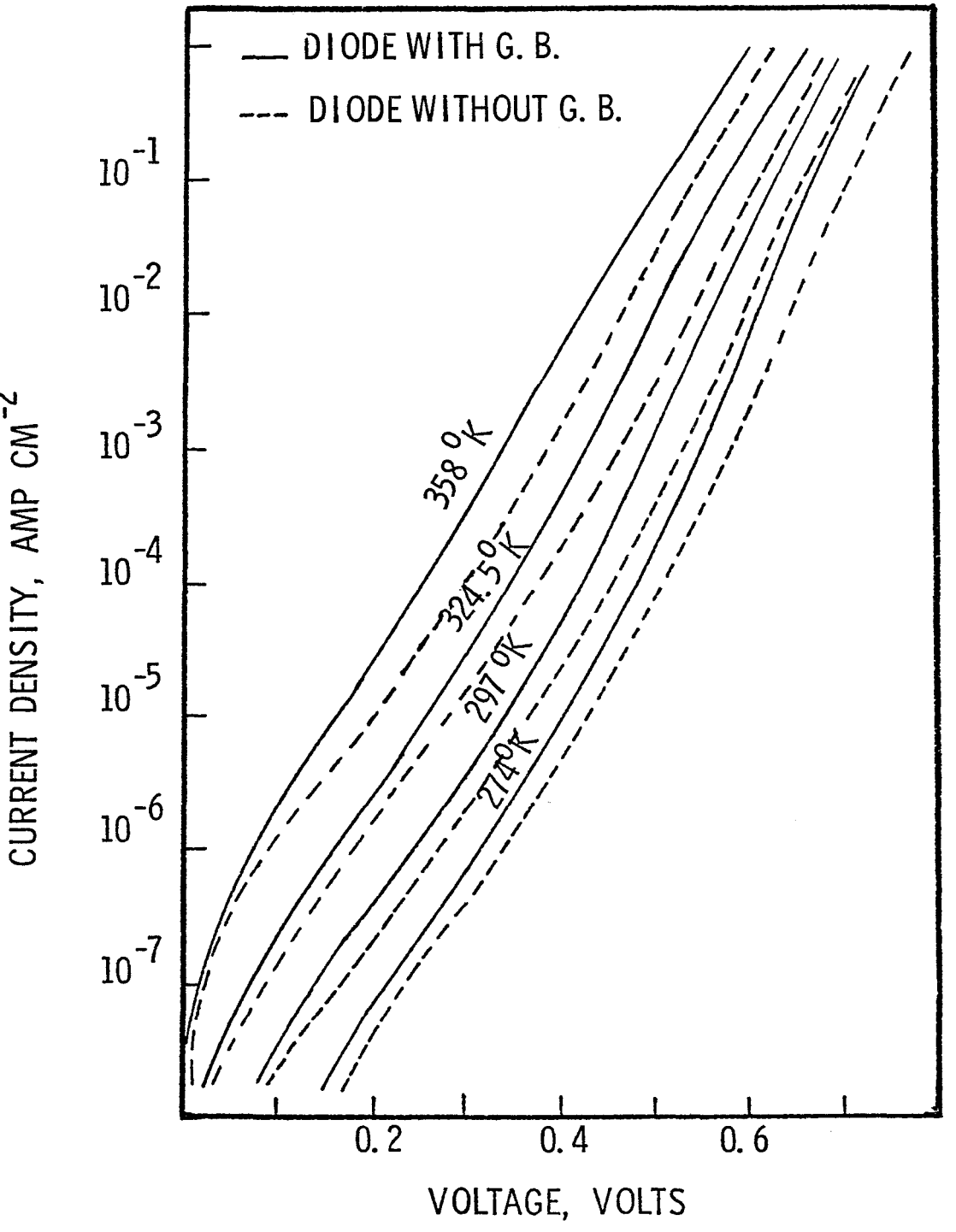

Fig. 16 The forward characteristics of a diode with a grain boundary (solid line) and a diode without grain boundaries at four temperatures.

The measured current voltage data of the diodes were fitted into the two exponential model:[19]

$$I = I_{01}[\exp(q\ V_D/kT) - 1] + I_{02}\ [\exp(q\ V_D/A_2kT) - 1] + \frac{V_D}{R_{sh}}$$

where the first two terms are the diffusion and recombination components, and the third term is the contribution of shunting. The V_D term includes the series resistance of the device, $V_D = V - IR_{ser}$. The computer program for the least square fitting, obtained through the courtesy of Dr. Richard J. Stirn of the Jet Propulsion Laboratory, was modified for use on the Cyber 72 computer at SMU. Five parameters, I_{01}, I_{02}, A_2, V_{sh}, V_{ser}, were calculated for each diode.

As an example, the parameters for diodes with and without grain boundaries shown in Fig. 16 and the root-mean-square deviation are summarized in Table III. In these diodes, the shunt resistance and series resistance made negligible contributions, and the root mean square deviation of the least square fitting is generally less than 5%. The room temperature parameters of five diodes without grain boundaries and nine diodes with grain boundaries in the same group are summarized in Table IV together with those of the single crystalline epitaxial diodes with similar resistivity and thickness of n- and p-regions. The I_{01} values of all diodes are of similar magnitudes. The I_{02} values of diodes without grain boundaries are very similar to those of single crystalline diodes; however, those of diodes with grain boundaries are distinctly higher. The high I_{02} values of diodes with grain boundaries indicate significant recombination of the grain boundaries.

The variation of I_{01} and I_{02} of the above group of diodes with and without grain boundaries with temperature is shown in Fig. 17. The activation energies for I_{01} are in the range 1.17 - 1.24 eV and 1.19 - 1.24 eV for

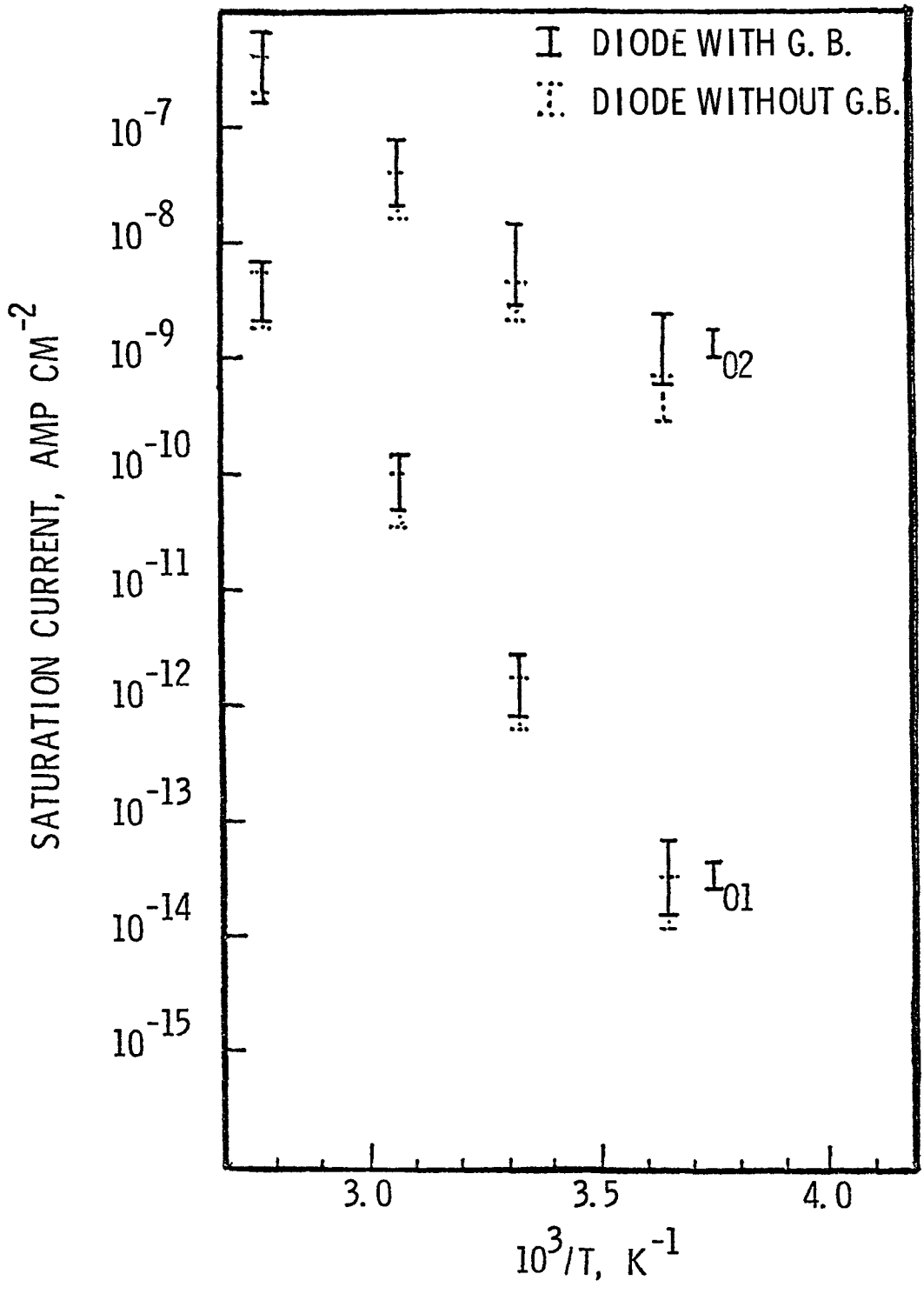

Fig.17 Saturation currents, I_{01} and I_{02}, of a group of diodes with and without grain boundaries as a function of temperature.

Table III. Parameters of the diode without grain boundaries and the diode with a grain boundary shown in Fig. 16.

TEMPERATURE °K		I_{01} Amp/cm^2	I_{02} Amp/cm^2	A_2	R_{ser} Ohm-cm^2	R_{sh} Ohm-cm^2	RMS
274	A	1.05×10^{-14}	2.61×10^{-10}	1.74	2.42×10^{-2}	1.11×10^{8}	2.58×10^{-2}
	B	4.50×10^{-14}	3.28×10^{-10}	1.65	2.58×10^{-2}	2.68×10^{7}	5.15×10^{-2}
297	A	5.77×10^{-13}	2.05×10^{-9}	1.70	2.37×10^{-2}	2.96×10^{6}	1.82×10^{-2}
	B	2.31×10^{-12}	2.43×10^{-9}	1.59	2.75×10^{-2}	1.37×10^{7}	5.08×10^{-2}
324.5	A	3.34×10^{-11}	1.64×10^{-8}	1.64	2.02×10^{-2}	1.23×10^{7}	1.31×10^{-2}
	B	1.19×10^{-10}	1.80×10^{-8}	1.47	2.57×10^{-2}	2.44×10^{6}	4.31×10^{-2}
358	A	1.99×10^{-9}	1.63×10^{-7}	1.57	1.29×10^{-2}	1.55×10^{6}	9.75×10^{-3}
	B	4.40×10^{-9}	1.48×10^{-7}	1.30	1.05×10^{-2}	3.26×10^{5}	2.82×10^{-2}

Table IV. Room temperature parameters of diodes with and without grain boundaries and single crystalline diodes (the p-region is of 0.1 ohm-cm resistivity)

	Diode without G.B.	Diode with G.B.	Single crystalline diode
I_{01}, Amp/cm^2	(0.6-1.7) x 10^{-12}	(0.8-2.6) x 10^{-12}	(1.2-2.0) x 10^{-12}
I_{02}, Amp/cm^2	(2 - 4) x 10^{-9}	(1.6-12) x 10^{-9}	(1.5-3.8) x 10^{-9}
A_2	1.69-1.74	1.62-1.80	1.55-1.70
Area, cm^2	0.06-0.08	0.6-1.2	0.1-0.15

both types of diodes, and those for I_{02} are in the range of 0.53 - 0.63 and 0.58 - 0.66 eV for diodes with grain boundaries and diodes without grain boundaries, respectively. Thus, these activation energies are similar to

the expected values, i.e., Eg for I_{01} and Eg/2 for I_{02}.

In conclusion, the dark current-voltage characteristics of a number of diodes with and without grain boundaries have been measured over a wide temperature range and fitted into the two exponential model. A comparison of the parameters indicates that while twin planes and grain boundaries do not affect the diffusion saturation current, the recombination saturation current in diodes with grain boundaries is distinctly higher. However, the recombination processes at grain boundaries appear to affect the forward characteristics only slightly and can be included in those in the space charge region without introducing a third exponential term. This is due to the small grain boundary length per unit area in the polycrystalline silicon p-n junctions deposited on unidirectionally solidified metallurgical silicon substrates.

VI. Polycrystalline Silicon Solar Cells

The principal approach developed in this program for the preparation of solar cells is to deposit the active region of the cell on partially purified and unidirectionally solidified metallurgical silicon substrate. Considerable efforts have been directed towards the development of various characterization techniques, such as minority carrier diffusion length, spectral response, photoresponse inhomogeneities, dopant profile, etc. The effects of grain boundaries and the reduction of grain boundary effects have also been investigated.

VI. 1. Preparation Technology

Solar cells of both n^+/p and p^+/n types with the configurations n^+-silicon/p-silicon/p^+-metallurgical silicon (acid-extracted)/graphite and p^+-silicon/n-silicon/n^+-metallurgical silicon(acid-extracted and phosphorus pentoxide treated)/graphite were prepared by the trichlorosilane process. The low resistivity substrate serves to minimize the contact resistance between silicon and graphite and also provides a back-surface field. The conductivity type and electrical resistivity of deposited silicon were controlled by using diborane or phosphine as a dopant, and the p-n junction was formed during the deposition process by varying the composition of the reactant mixture. Typically, 20-30 μm of 0.2-0.5 ohm-cm p-type (or n-type) silicon was deposited at 1100°-1150°C at a rate of about 1 μm/min followed by the deposition of 1.5-2 μm of 0.002-0.004 ohm-cm n-type (or p-type) silicon at a rate of about 0.2 μm/min. In some cases, a graded profile in the upper region has been used to provide a drift field. The deposit is usually epitaxial with respect to the substrate as shown by metallographic examinations. The sheet resistance of the surface-layer, measured by the four

point probe technique, was 30-60 ohms/square. The solar cell structure was annealed in many cases before further processing.

The graphite plate serves as the ohmic contact to the base region. The grid contact to the front surface, 4 lines per cm, was made by evaporating about 1000 Å of titanium and 3-5 μm of silver to the cell surface through a metal mask, followed by annealing in a hydrogen atmosphere at 500°C. Subsequently, silver was electrodeposited onto the grid lines to increase their thickness, and anti-reflection coatings of silicon dioxide or tin dioxide were applied by chemical vapor deposition. The configuration of a polycrystalline silicon solar cell is shown schematically in Fig. 18.

VI. 2. Dopant Profile

The concentration and distribution of electrically active impurities in a solar cell are important factors determining its characteristics. For example, the spectral response of an n^+/p solar cell in the short wavelengt region is strongly dependent on the thickness of, and dopant profile in, th n^+-region. The short wavelength response cannot be optimized without a detailed knowledge of the properties of the n^+-layer.

The spreading resistance technique was used to determine the resistiv profile in polycrystalline solar cells. Attempts were made to measure the resistivity profile by grooving the surface of the cell and applying the spreading resistance probe to the grooved surface. Although the profile in the base-region can be measured, the surface-region could not be detected even with shallow grooves because of its small thickness. Thus, the standa technique of applying the spreading resistance probes to the beveled surfac cf solar cells was investigated. Measurements of thin films, 1 μm or less in thickness, require special techniques to obtain accurate depth and dopan

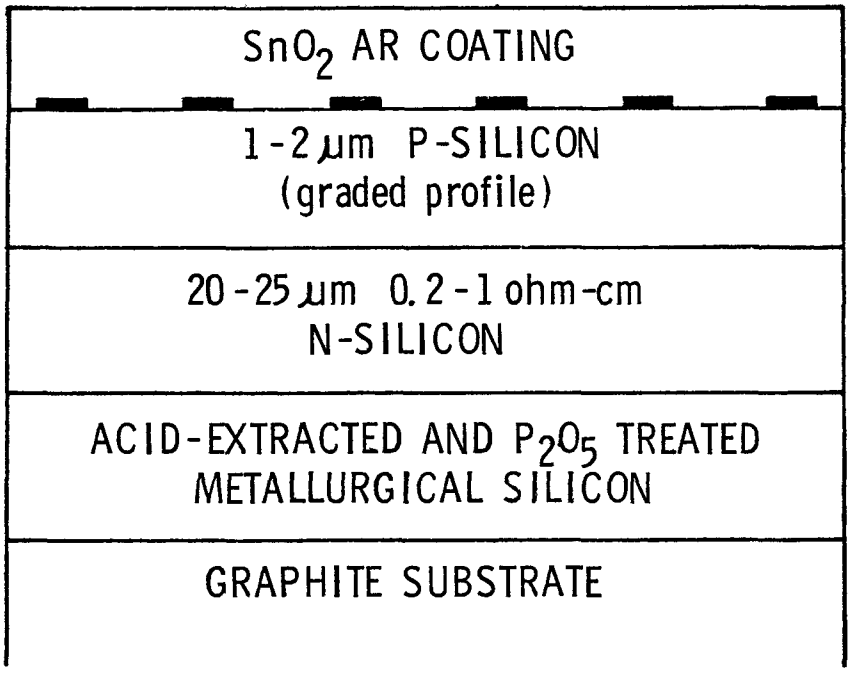

Fig. 18 Configuration of a polycrystalline silicon solar cell.

profile. The bevel angle must be small and accurately known, the bevel edges must be clearly defined, and a single probe should be used to obtain the highest possible spatial resolution.

The polishing of silicon specimens at small angles (20' for example) with sharp bevel edges requires a hard protective surface coating to prevent the edge rounding. Prior to the polishing process, a silicon nitride film of 0.3-0.5 μm thickness was deposited on each specimen at about 800°C by the reaction of ammonia and silane in a gas flow system. The large hardness of silicon nitride eliminated the rounding of the edge and probe punch through, and its high electrical resistivity accurately defined the position of the surface of the specimen on the spreading resistance profile. Slow mechanical polishing was carried out using QUSO-32, a very fine silicon dioxide abrasive, on a lucite plate to minimize scratches.

Single probe measurements were made to eliminate errors due to misalignment of the probes with the bevel edge. One probe contacted the specimen directly, and the second probe contacted a Ga-In alloy strip ultrasonically soldered across the n+/p/p+ or p+/n/p+ structure.

VI. 3. Current-Voltage Characteristics

Solar cells prepared in this work were 9 - 30 cm^2 in area. Their current-voltage characteristics were measured at room temperature in the dark and under illumination. Smaller area cells usually exhibit better characteristics. Figure 19 shows the current-voltage characteristics of the best solar cell of 9 cm^2 area at 28°C under illumination equivalent to AM1 conditions. Illumination was provided by four individually adjustable, with respect to both the position and intensity, GE ELH quartz-halogen lamps (300 W each), and the intensity distribution over

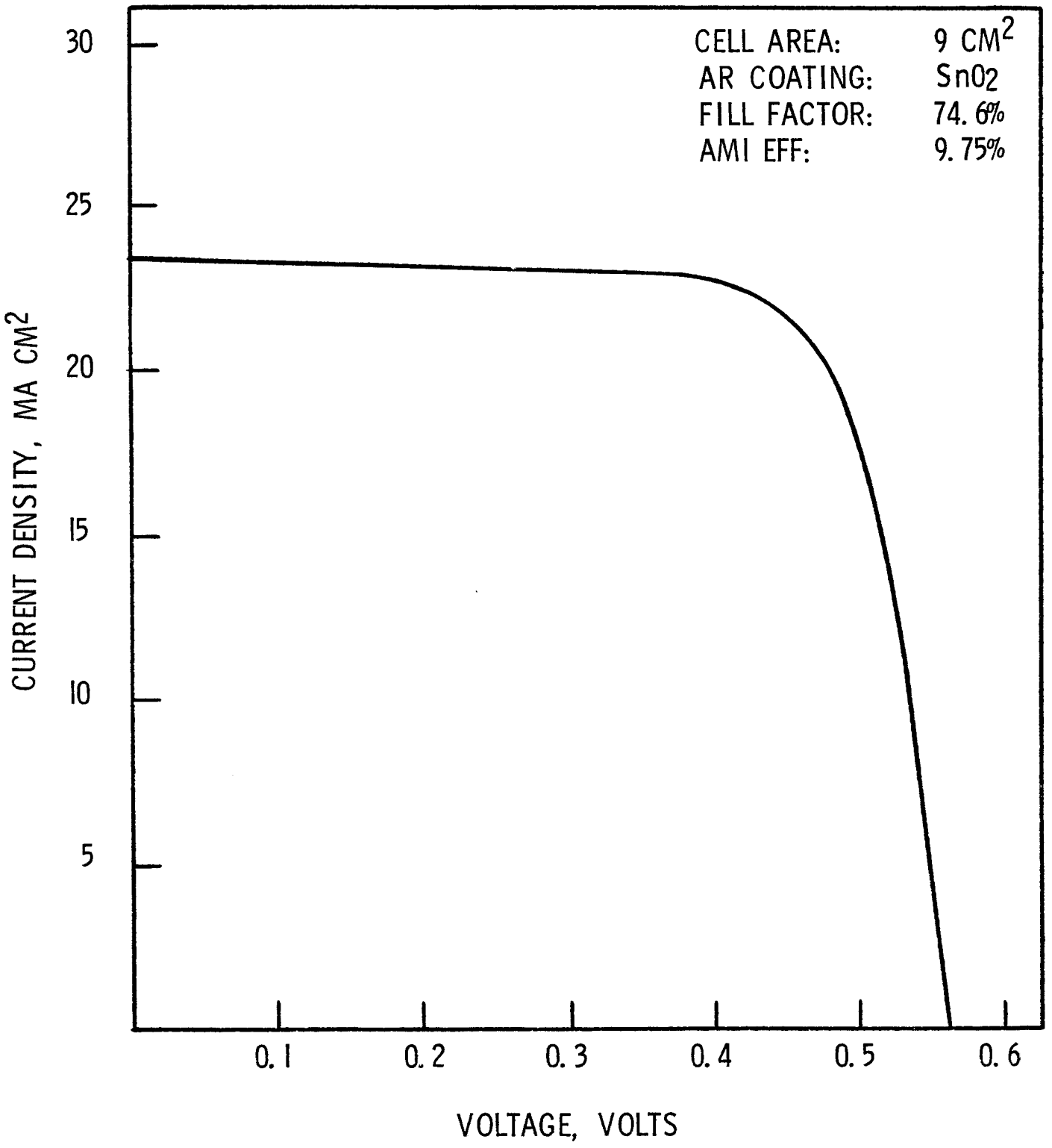

Fig. 19 Current-voltage characteristics of a thin film polycrystalline silicon solar cell under illumination with GE ELH quartz-halogen lamps equivalent to AM1 conditions.

the active area of cells was within ± 2%, in accordance with the proposed testing standards adopted at the ERDA/NASA Terrestrial Photovoltaic Measurement Workshop in November 1976. The open-circuit voltage, short-circuit current density, and fill factor are 0.564V, 23.2 mA/cm, 74.6%, respectively, corresponding to a conversion efficiency of about 9.75%.

VI. 4. Spectral Response

An apparatus for the measurement of spectral response of solar cells has been constructed using eleven interference filters with peak transmission at 0.4, 0.45, 0.5, 0.6, 0.7, 0.8, 0.85, 0.9, 0.95, 1.0, and 1.014 μm; the filters had a 100 Å band pass at half maximum. The spectral response of a solar cell is measured in terms of the short-circuit current, in milliamperes, divided by the incident optical power, in milliwatts, at a specific wave length. The intensity of light incident on the solar cell was determined by measuring the ratio of the short-circuit current of the cell under test and the short-circuit current of a calibrated cell of known spectral response. The calibrated cell was obtained from the Lewis Research Center of the National Aeronautics and Space Administration. The efficiency of this cell under AM0 and AM1 conditions and its absolute spectral response characteristics were measured at the Lewis Research Center.

Since the spectral response of a solar cell may vary under different levels of ambient light, regardless of the actual spectrum of the incident light, a constant source of white light in addition to the monochromatic light is required to measure this variation. In the present system, white light from two 300 W GE ELH lamps is directed onto the solar cell independently of the monochromatic illumination. This allows the spectral response to be measured under near AM0, AM1, or other illumination conditions. Separation of the signals due to the monochromatic light and the constant

bias light is achieved by mechanically chopping the monochromatic light and measuring the a.c. component of the signal with a lock-in amplifier.

The spectral response of many polycrystalline silicon solar cells has been measured using a calibrated single crystalline silicon solar cell as a reference. The calibrated cell is 2 cm x 2 cm in area, and the active area of the polycrystalline cell is made to the same size by masking. Figure 20 shows the spectral response of a polycrystalline silicon solar cell together with that of a calibrated cell for comparison. The peak response for the polycrystalline cell occurs at a shorter wavelength than that for the single crystalline cell. In addition, the quantum efficiency in the polycrystalline solar cell is lower than that in the single crystalline cell. The shift in peak response and lower quantum efficiency is not unexpected in view of the small thickness of the active region of, and the short minority carrier diffusion length in, the polycrystalline cell. The apparent decrease in short wavelength response indicates a high recombination velocity in or near the n^+ layer.

The spectral response of polycrystalline silicon solar cells has also been measured under light bias. An example is shown in Fig. 21. The spectral response of the cell is essentially unchanged under AM0 light bias except near the peak region (the apparently high response at 400 nm is in error due to the extremely low signal to noise ratio). The small change in spectral response brought about by the light bias is in accord with the results (cf. VI.5) that the minority carrier diffusion length in polycrystalline silicon solar cells remained essentially the same under various levels of light bias. In contrast, many single crystalline silicon solar cells show both an increase in diffusion length

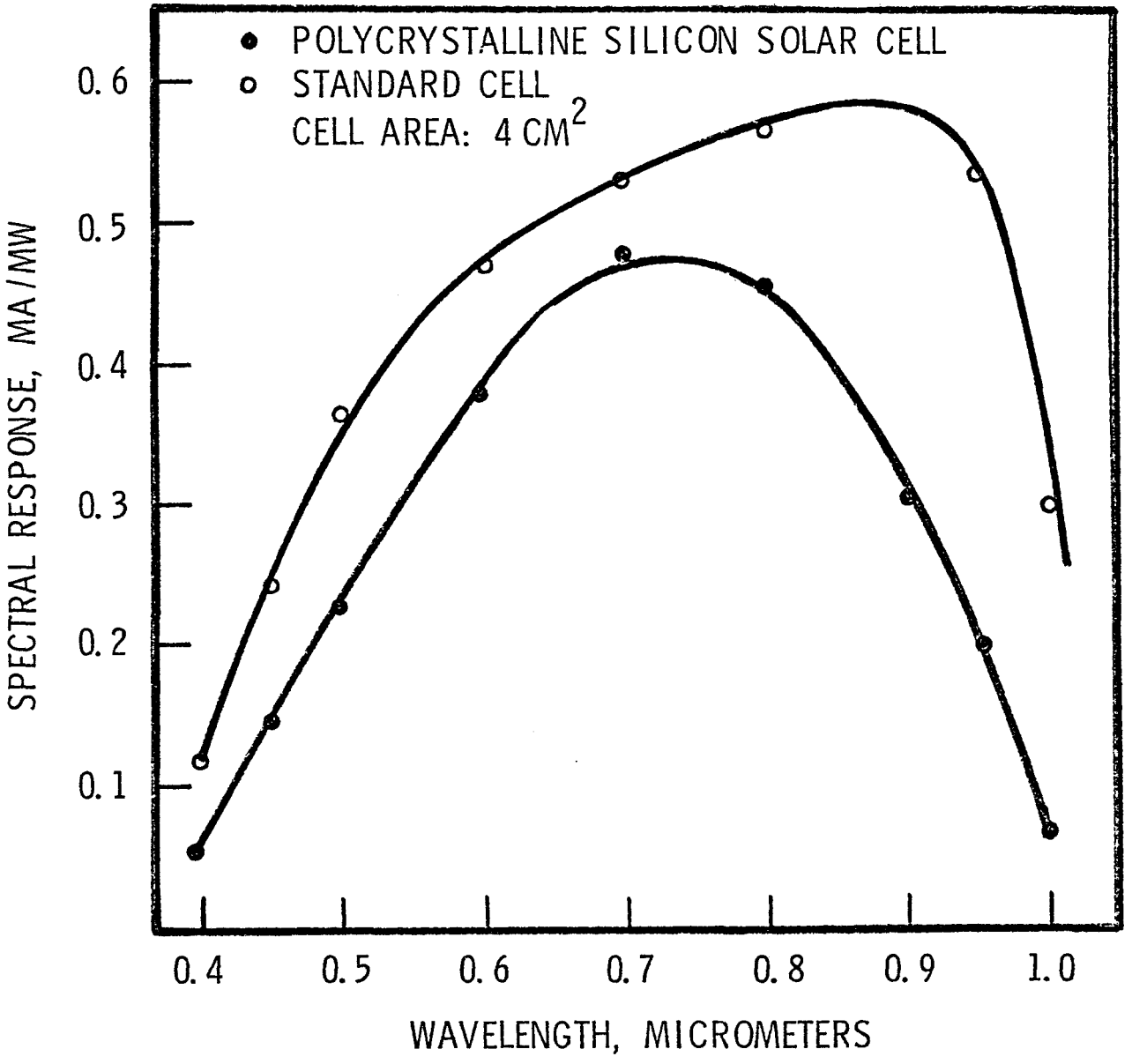

Figure 20 Spectral response of a thin film polycrystalline silicon solar cell in comparison with a calibrated single crystalline silicon solar cell.

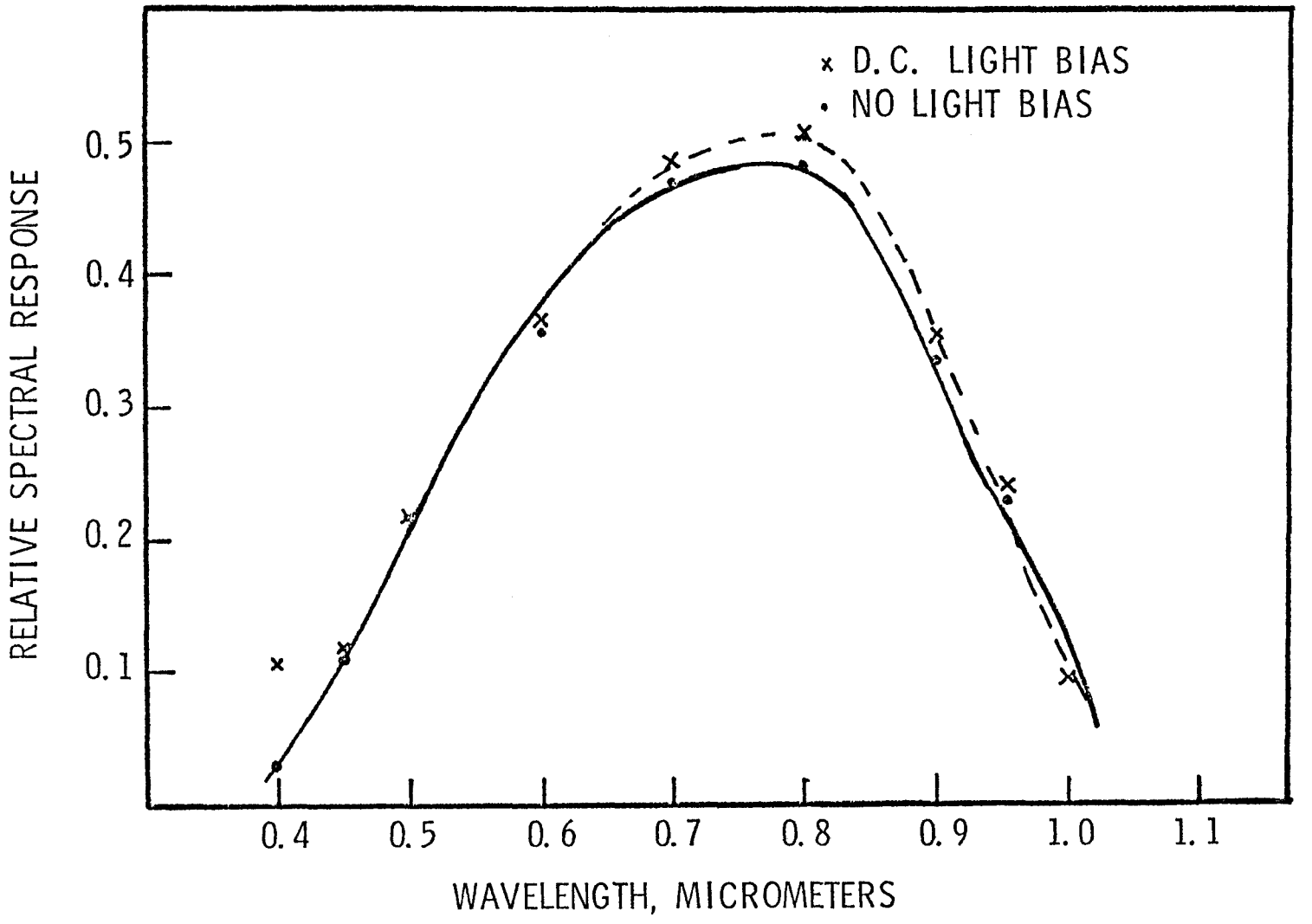

Fig. 21 Spectral response of a polycrystalline silicon solar cell under AM0 light bias.

and in relative spectral response under illumination.

VI. 5. Minority Carrier Diffusion Length

The minority carrier diffusion length is the most important parameter affecting the conversion efficiency and spectral response of solar cells. The steady state surface voltage method has been used for the determination of minority carrier diffusion length in semiconductors.[20-23] In this method, the surface of a semiconductor is illuminated with chopped monochromatic radiation with energy slightly higher than the energy gap of the semiconductor. The photo-generated electron-hole pairs diffuse to the surface and are separated by the electric field of the depletion region to produce a surface photovoltage, V_{sp}. When the semiconductor is of p-type conductivity, the magnitude of V_{sp} is a function of the excess electron density, Δn, injected into the surface depletion region. The excess electron density depends on the incident light intensity F, the reflection coefficient R, the quantum efficiency η, the optical absorption coefficient α, the electron diffusion coefficient D, the electron diffusion length L, and the surface recombination velocity S. If $d_1 \ll L$, $d \gg L$, $\alpha d_1 \ll 1$, $\alpha d \gg 1$, and $\Delta n \ll P_0$ (where d_1 and d are, respectively, the depth of the space charge layer and the sample thickness), it has been shown that Δn can be expressed by the following equation:

$$\Delta n = \frac{F\eta(1 - R)\ \alpha L}{[(D/L) + S](1 + \alpha L)} \qquad (1)$$

To determine L, the surface photovoltage is measured as a function of the wavelength, and the incident light intensity is adjusted to produce the same value of V_{sp}. If η and R are assumed to be constant over the wave-

length range under consideration, light intensity is a linear-function of the reciprocal absorption coefficient for each wavelength, i.e.

$$F = \text{constant } (\alpha^{-1} + L) \qquad (2)$$

Thus, the extrapolation of the F versus α^{-1} plot to zero intensity yields L as the negative intercept.

The surface photovoltage method has also been extended to shallow junction devices, such as solar cells.[24] Since the junction depth is considerably smaller than the diffusion length, the open-circuit voltage V_{oc} rather than V_{sp} is measured as a function of the wavelength, and the incident light intensity required to produce a given V_{oc} is determined. The extrapolation of the F versus α^{-1} plot to zero intensity also yields L. The open-circuit voltage technique is convenient for the measurement of L. The V_{oc} of an illuminated solar cell is given by:

$$V_{oc} = \frac{kT}{q} \ln\left(\frac{I_{sc}}{I_s} + 1\right) \qquad (3)$$

where I_{sc} and I_s are short-circuit current and saturation current, respectively. Thus, low illumination levels to produce V_{oc} of 20 mV or less is necessary so that V_{oc} is essentially a linear function of I_{sc} or light intensity. At high illumination levels, a small error in setting V_{oc} may result in a large error in the light intensity.

In this program, the surface photovoltage method is extended by using I_{sc} for the measurement of collection of photogenerated carriers. Since I_{sc} is a linear function of light intensity up to relatively high illumination levels, diffusion length measurements can be extended to injection levels encountered under AM0 conditions. The justification

of using I_{sc} for the collection of photogenerated carriers is briefly as follows. The current produced by a solar cell under illumination is given by:

$$I = I_J - I_L \qquad (4)$$

where I_L is the photocurrent, and I_J is the junction current flowing in the opposite direction. At low voltages, 10 mV or less, the junction current is negligible, and the measured current is essentially the photo current which is the sum of contributions from the n-region, the p-region, and the depletion region. When a shallow junction n^+/p solar cell is illuminated with monochromatic radiation of low absorption coefficients, such as that in the wavelength range 0.8 to 1.03 μm for silicon, the contributions due to the n-region and depletion regions may be neglected. The short-circuit current due to the p-region is given by:[25]

$$I_{sc} = \frac{qF_o\alpha L}{\alpha^2 L^2 - 1} [\alpha L e^{-\alpha t} - e^{-\alpha t} \text{ Coth}(d/L) + e^{-\alpha(d+t)} \text{ Cosech}(d/L)] \quad (5)$$

where F_o is the intensity incident into the surface, and t is the junction depth. When $d \geq 2L$ and $\alpha d \geq 1$, the term $e^{-\alpha d}$ cosech (d/L) becomes negligible, and Coth(d/L) approaches unity. Equation (5) can then be written as:

$$I_{sc} = \frac{q F_o L e^{-\alpha t}}{\alpha^{-1} + L} \qquad (6)$$

If the intensity incident on the base region, $F = F_o e^{-\alpha t}$, is adjusted to maintain a given I_{sc} for all wavelengths, then Equation (6) is reduced to

$$F = K(\alpha^{-1} + L) \qquad (7)$$

where K is a constant depending only on cell parameters and the particular

value of I_{sc} selected. The effects of a back surface field, trapping, etc., have not been considered. However, the SPV technique has been shown to be valid for epitaxial layers of thicknesses $\geq$ 4L. If this condition is met, the back surface field could be ignored.

A schematic diagram of the apparatus for the measurement of minority carrier diffusion length is shown in Fig. 22. The specimen surface is illuminated with monochromatic radiation from a quartz-halogen lamp chopped at 13 Hz. Focusing optics may be used to vary the size of the illuminated area on the specimen. When the specimen is in the form of a slice, the surface photovoltage generated is capacitively coupled into a lock-in amplifier for measurement. For solar cells, the short-circuit current is measured by the voltage drop across a 10 ohm resistor. The intensity of incident light is controlled by varying the voltage of the light source and is measured by a radiation detector calibrated with a thermopile. It is adjusted to produce the same V_{sp} or I_{sc} at various wavelengths of illumination. A constant white light with an irradiance greater than 135 mW/cm^2 may be used for light bias. The measurement is usually carried out from the shortest wavelength. After the measurements are completed, the first measurement is repeated, and a reproducibility of $\pm$ 5% is considered acceptable. Otherwise, the entire measurements are repeated until a reproducibility of $\pm$ 5% is obtained. The poor reproducibility occurs essentially in the case of silicon slices and can be attributed to changes in the surface states of the specimen. This problem is most severe immediately after etching the surface of the specimen or removing the surface oxide with hydrofluoric acid. At a constant light intensity, the surface photovoltage may decay or increase exponentially

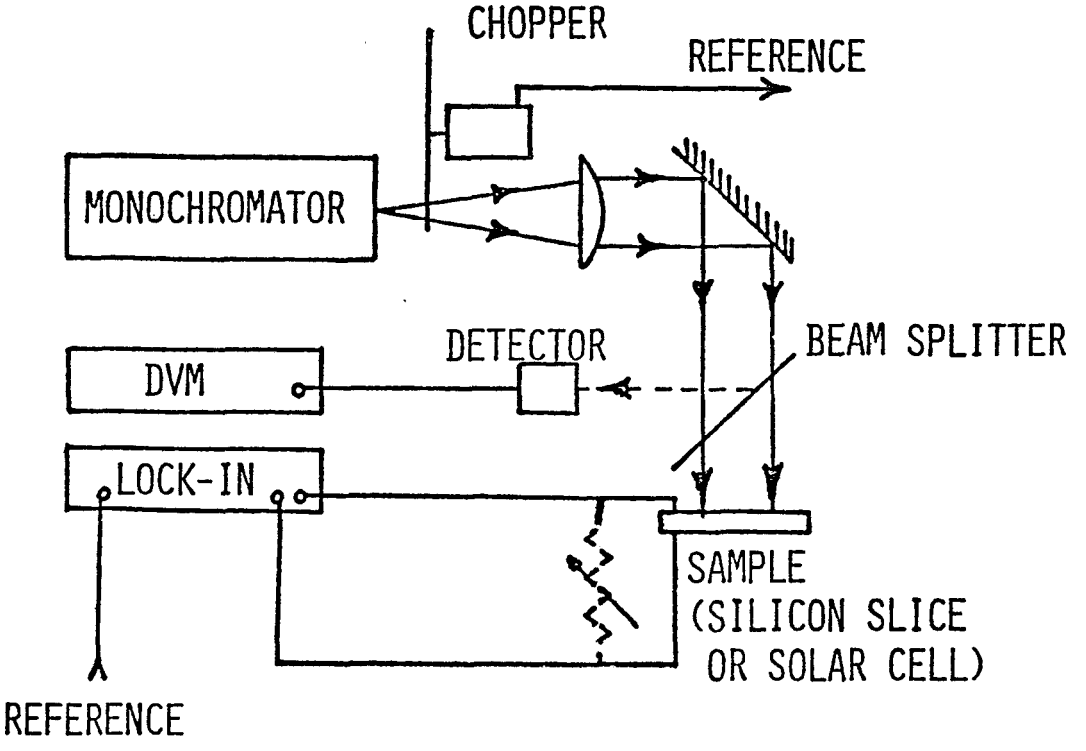

Fig. 22 A schematic diagram of the apparatus for the measurement of minority carrier diffusion length.

with time constants of up to several minutes. Specimens exhibiting this type of behavior are allowed to stabilize before measurements. For solar cells where the surface states play a much smaller role in signal level, the reproducibility problem is almost nonexistent. The absorption coefficients of silicon at various wavelengths are calculated from the known data for stress relieved silicon.[26]

To verify the validity of Eq. (7), the minority carrier diffusion length in a thin film polycrystalline silicon solar cell was measured by the I_{sc} method and compared with that obtained by the standard SPV method. The plots of relative intensity versus α^{-1} for the three collection techniques are shown in Fig. 23. Curve A is the constant SPV plot for the solar cell. Curve B is for constant short-circuit current, and Curve C is for constant V_{sp} with the upper layer removed by chemical etching. The three collection techniques yield essentially the same diffusion length within the experimental accuracy. The measurements of minority carrier diffusion length by the short-circuit collection method has been applied to a large number of polycrystalline silicon solar cells. An example is shown in Fig. 24, where three different light intensities were used to show the independence of the measured diffusion length on light intensity. The measured diffusion length in most polycrystalline silicon solar cells is in the range of 15 to 30 μm. Since the thickness of the base region is usually 20-30 μm, the effect of the back-surface field could be appreciable, and the measured diffusion length is an "effective" diffusion length. The effective diffusion length in the base region of several polycrystalline silicon solar cell has also been measured as a function of the d. c. light bias applied to the cell. The light bias was obtained from a 150 W Xenon

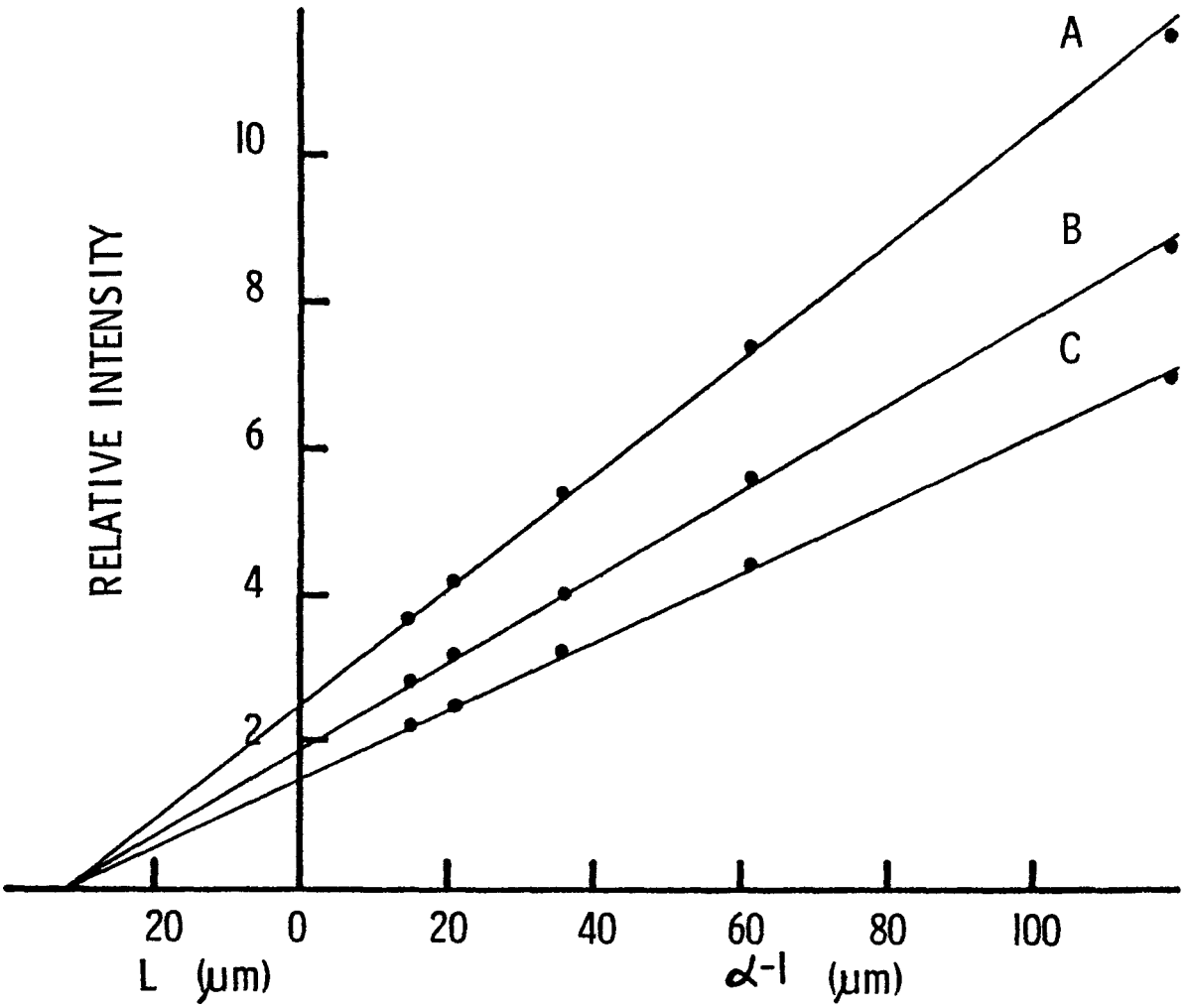

Fig. 23 Diffusion length data for a thin film polycrystalline silicon solar cell by different collection methods.

A. Capacitive coupled SPV data
B. Constant short-circuit current data
C. Capacitive coupled SPV data after the removal of the upper layer

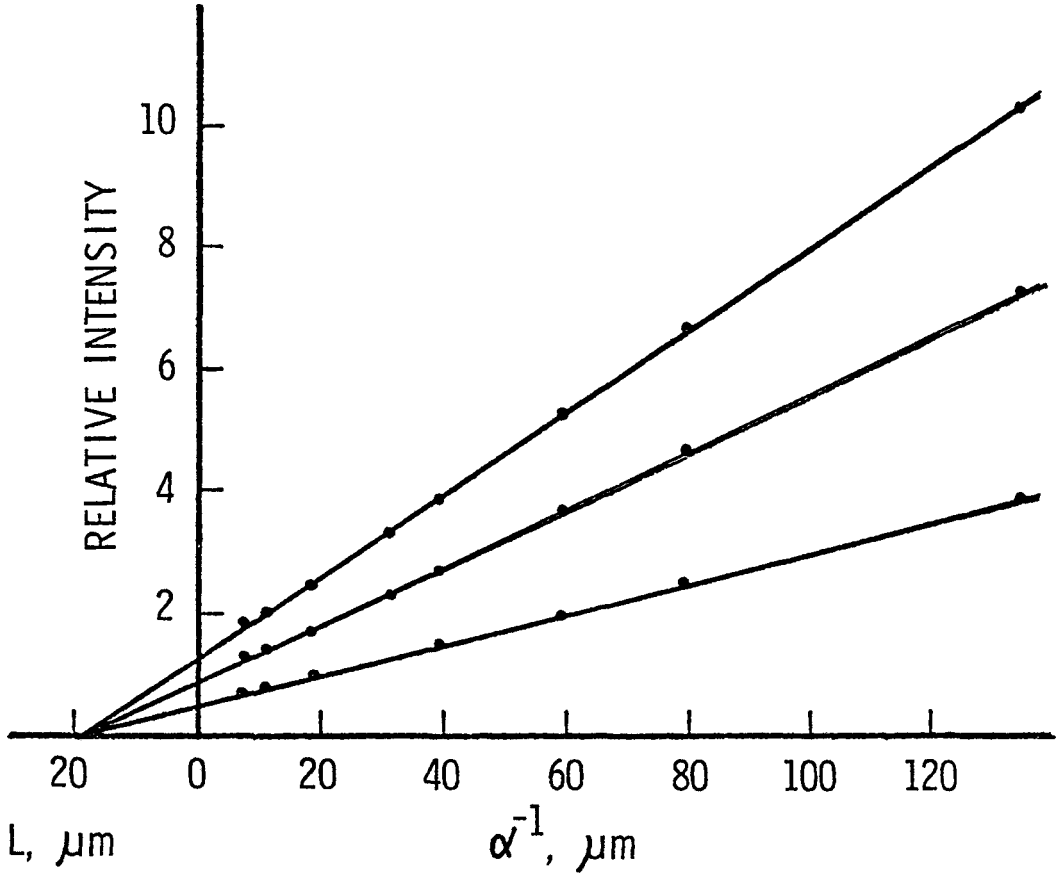

Fig. 24 Diffusion length data for a polycrystalline silicon solar cell at different illumination levels.

high pressure arc lamp coupled to the cell via a 1/8" diameter optical light guide. The area of the cell used for the measurement was 4 cm^2 including the grid pattern. An example is shown in Figure 25 where the effective diffusion length in a polycrystalline silicon cell is plotted as a function of the short-circuit current due to the d. c. light bias. The effective diffusion length remained essentially unchanged, while the diffusion length in single crystalline silicon solar cells increased slightly under light bias.

Experiments have also been carried out to measure the effective local diffusion length or diffusion length profile in polycrystalline silicon solar cells. The surface of the cell was masked with black wax to expose selected regions of 0.5-1 mm^2 in area. The diffusion length measurements were carried out at 2 mm intervals by the short-circuit current collection method. Figure 26 shows the diffusion length profile across the width of a polycrystalline silicon solar cell, where the diffusion length inhomogeneities are apparent, and the decrease in diffusion length is most pronounced at structural defects.

VI. 6. Photoresponse Scanning

The measurement of photoresponse profile of a solar cell provides information on its electrical and structural uniformity. One solar cell has been examined by Dr. David E. Sawyer of the National Bureau of Standards using his laser scanner at 0.633 μm and 1.15 μm. [27] Two display screen photographs were made for each of the selected wavelength and bias conditions: one for the "z-axis", or beam intensification display mode commonly used with cathode ray tubes, and one for the "y-deflection" mode in which a horizontal scan line is deflected upward an amount proportional to the

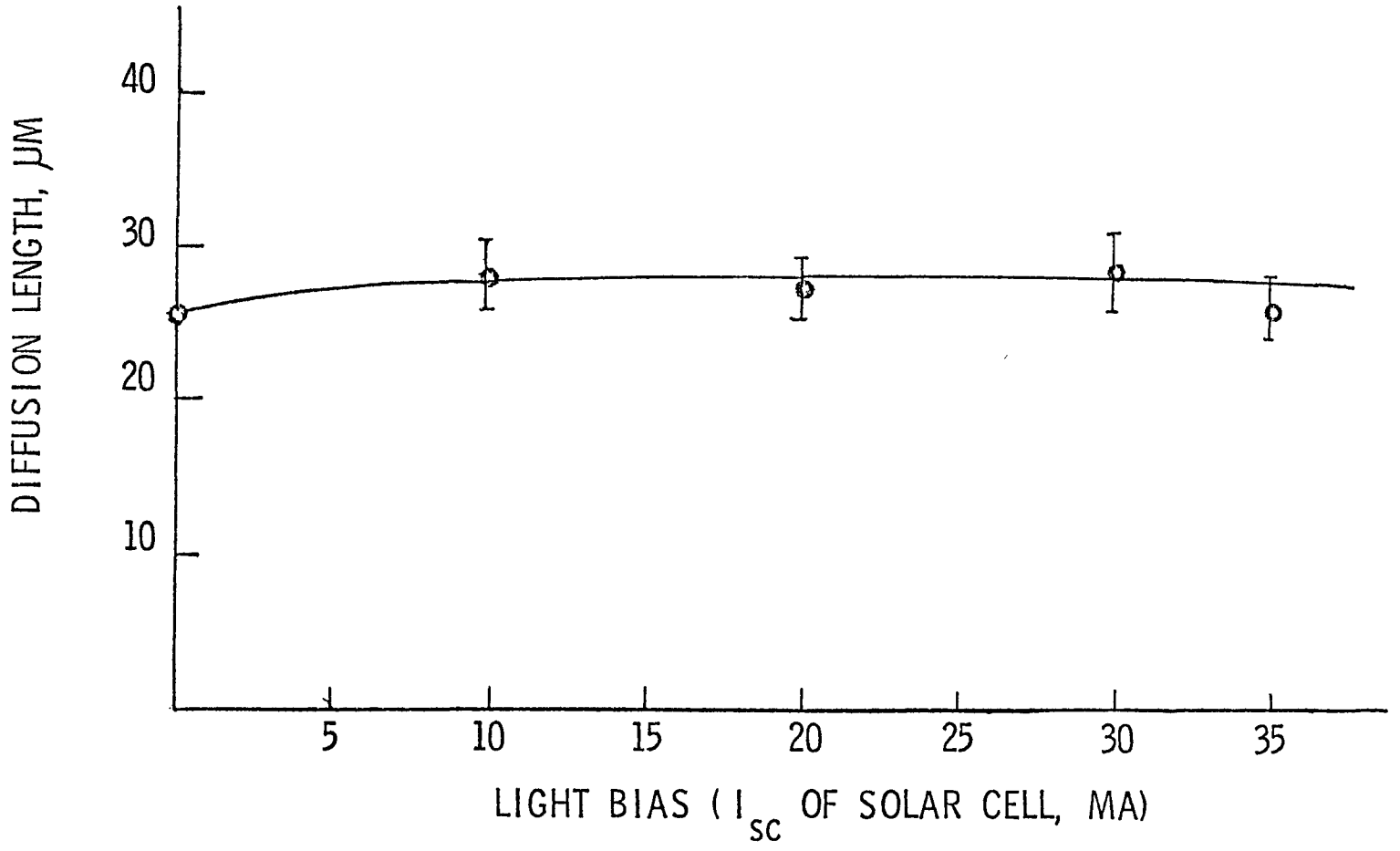

Fig. 25 Effective diffusion length in the base region of a polycrystalline silicon solar cell as a function of light bias.

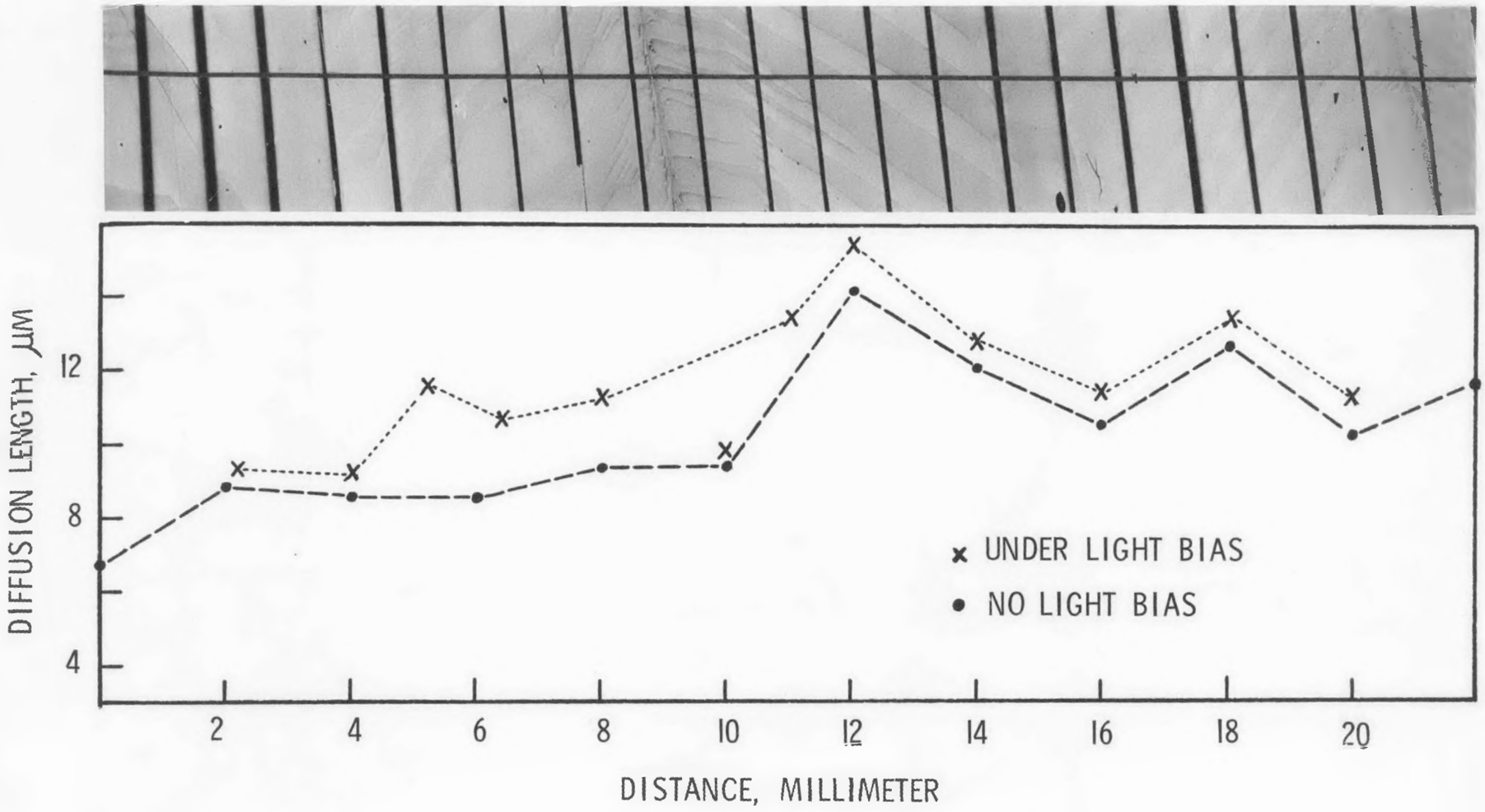

Fig. 26 Diffusion length profile across the width of a thin film polycrystalline silicon solar cell.

instantaneous amplitude of the signal. The former is useful for getting a general picture of the cell's photoresponse, but the latter is better for quantifying the results. Figure 27 shows the photographs of the 0.633 μm and 1.15 μm scanned photoresponse at zero bias, and Figure 28 shows the photographs of the 0.633 μm scanned photoresponses at 50 mA and 100 mA bias. The cell load was essentially a short-circuit for ac, and the zero bias 0.633 μm photographs was interpreted as maps of the short-circuit small-signal photocurrent at that wavelength. This photoresponse appears to be quite uniform, after one takes into account metallization and other artifacts. By scanning at the same wavelength and load but with the cell forward-biased, fabrication-related defects such as metallization regions making poor contact with the cell were detected. Occasionally forward-biasing produces cell noisebursts which mask the photoresponse. The cell under investigation, however, was well-behaved and quiet for all biases imposed and this was considered as a confirmation of its basically good quality. But, metallization areas which did not make ohmic contact were detected. These show up by a lowered photoresponse in their neighborhoods. These areas could cause the cell's fill factor to be less than it might be otherwise. At 1.15 μm, the solar cell had weak photosignals due to lower absorption coefficient. Nevertheless, good signal-to-noise ratios were observed. The overall response was also found to be reasonably uniform.

To determine local variations in spectral response and diffusion length in thin film solar cells and to correlate these variations with structural defects, a photoresponse scanner using gallium-aluminum arsenide lasers with wave lengths at 8051, 8251, and 8850 Å was constructed. The advantage of the photoresponse scanning technique is that the depth of

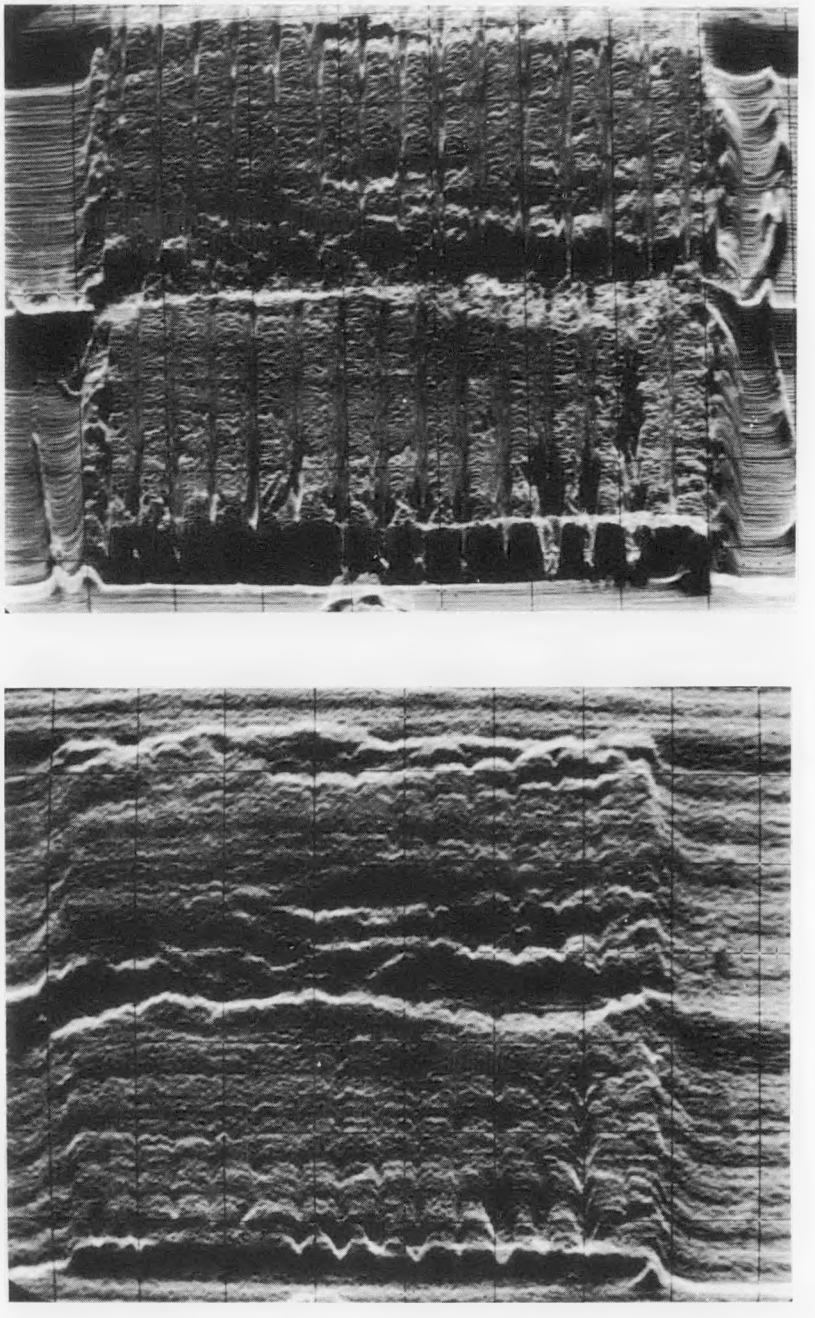

Fig. 27 Laser scanned photoresponse of a thin film polycrystalline silicon solar cell at 0.633 μm (upper) and 1.15 μm (lower) under zero bias.

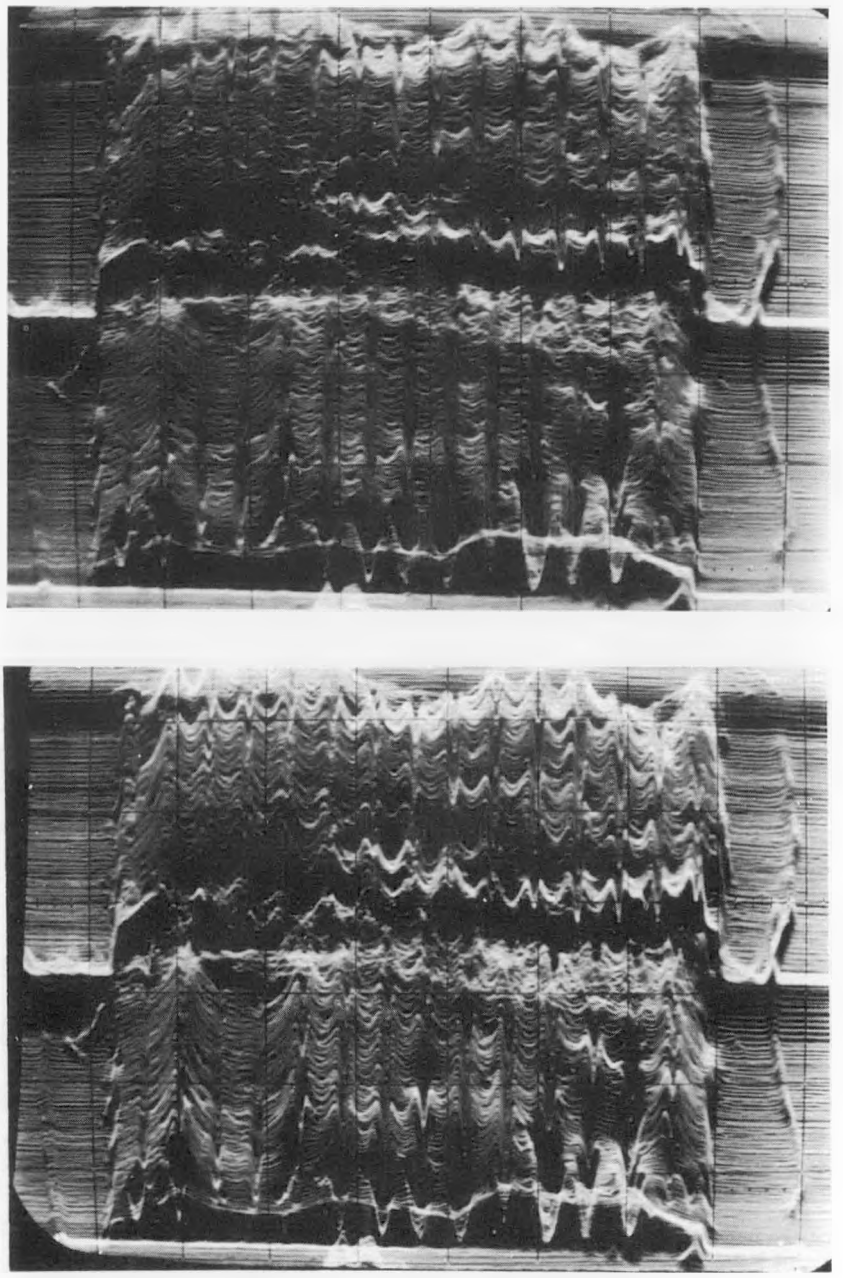

Fig. 28 Laser scanned photoresponse of a thin film polycrystalline silicon solar cell at 0.633 μm under 50 mA (upper) and 100 mA (lower) bias.

carrier generation can be varied by varying the wavelength of the incident radiations. The depth of carrier generation in silicon by 8051, 8251, and 8860 Å radiation are approximately 11.8, 14.2, and 26.3 μm, respectively. A comparison of the scanned response at the three wavelengths will allow semiquantitative evaluation of the changing process parameters in solar cell fabrication and of the effectiveness of grain boundary passivation techniques.

The external quantum efficiency, Q, for carrier collection by the base region of a solar cell is given approximately by the relation

$$Q = L\, e^{-\alpha t} / (L + \alpha^{-1})$$

where L is the minority carrier diffusion length in the base region, α is the absorption coefficient of the incident light, and t is the junction depth. The effects of a defect region with a low effective diffusion length on the photoresponse can be calculated. If the diffusion length in the base region is ℓ_1 and the effective diffusion length in the defect region is ℓ_2, the output in the defect region relative to the matrix can be calculated when the defect region is considerably larger than ℓ_2 in dimensions. Figure 29 shows the photoresponse modulation produced by a given diffusion length modulation as a function of the reciprocal absorption coefficient of incident radiation. It is assumed that in curves A and C, ℓ_1 = 120 μm and ℓ_2 = 80 μm and 40 μm, respectively, and that in curves B and D, ℓ_1 = 30 μm and ℓ_2 = 20 μm and 10 μm, respectively. These results indicate that solar cells with shorter diffusion length are more strongly affected by diffusion length reducing defects and that all cells are affected more strongly in the long wavelength region. Figure 30 shows the ratio of photoresponse as a

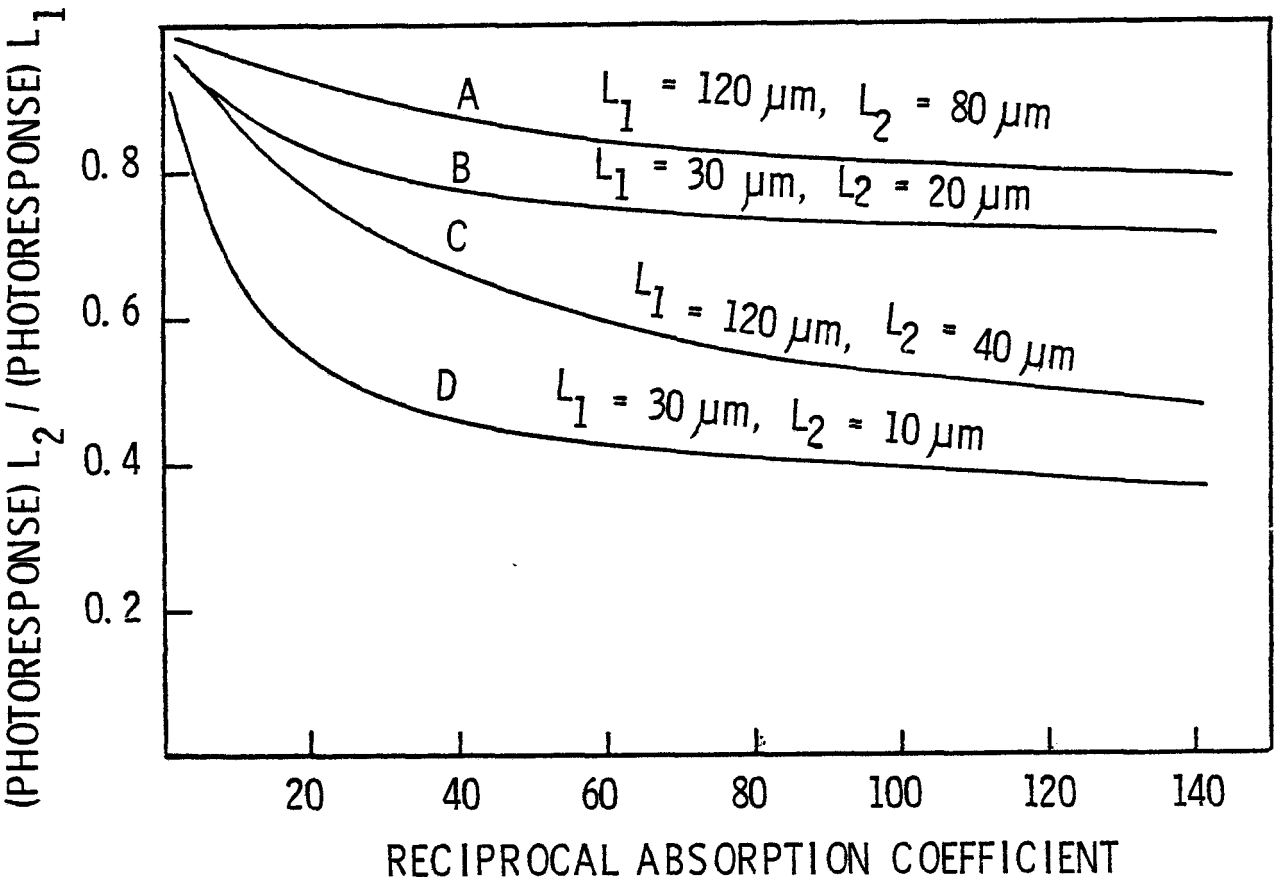

Figure 29 Photoresponse modulation due to diffusion length modulation as a function of reciprocal absorption coefficient.

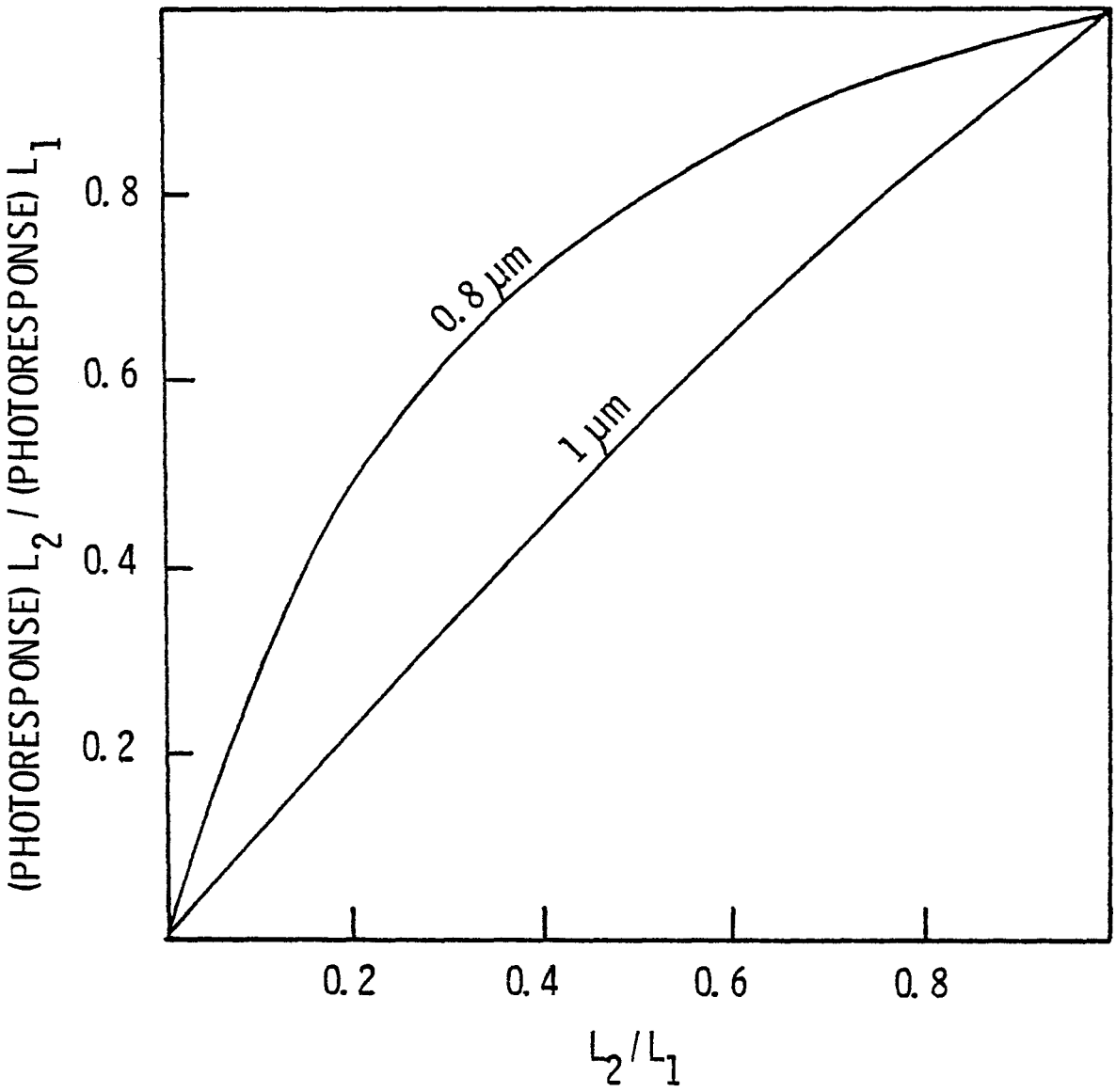

Figure 30 Photoresponse modulation as a function of the diffusion length ratio ℓ_2/ℓ_1 at ℓ_1 = 30 μm.

function of the ratio of diffusion length ℓ_2/ℓ_1, at a fixed ℓ_1(30 μm) and at two wavelengths 0.8 and 1 μm. This ratio varies with $\ell_2(\ell_1 + \alpha^{-1})/\ell_1(\ell_2 + \alpha^{-1})$. At long wavelength, $\alpha^{-1} >> \ell_1$, the modulation of the photoresponse is essentially a linear function of local diffusion length.

Figure 31 shows the photoresponse scan across the width of a polycrystalline silicon solar cell using 8251 Å radiation. Variations of the short-circuit current with position are apparent, and all irregularities can be correlated with visible defects on the cell surface.

VI. 7. Stability of Thin Film Silicon Solar Cells

Thin film polycrystalline silicon solar cells are prepared at relatively high temperatures (1100°C) and are expected to have an inherent stability similar to that of single crystalline silicon solar cells. To verify their expected stability, preliminary work concerning the effects of temperature, humidity, and optical stress on several thin film silicon solar cells has been carried out. Lead wires were soldered to the grid on the front surface through tin oxide film by ultrasonic soldering and were attached to the graphite by a metal screw. In some cases, a copper-constantan thermocouple was also soldered to the grid for the measurement of cell temperature. The cell was then encapsulated in GE RTV 615 transparent silicon potting compound, and SS-4120 primer was used to insure a strong bond between the cell and the silicon.

The current-voltage characteristics of thin film polycrystalline silicon solar cells were measured in the temperature range of -40° to 100°C in the dark and under illumination with ELH quartz-halogen lamps at AM1 conditions. The solar cells were of 10-30 cm^2 in area. The AM1 efficiency of 30 cm^2

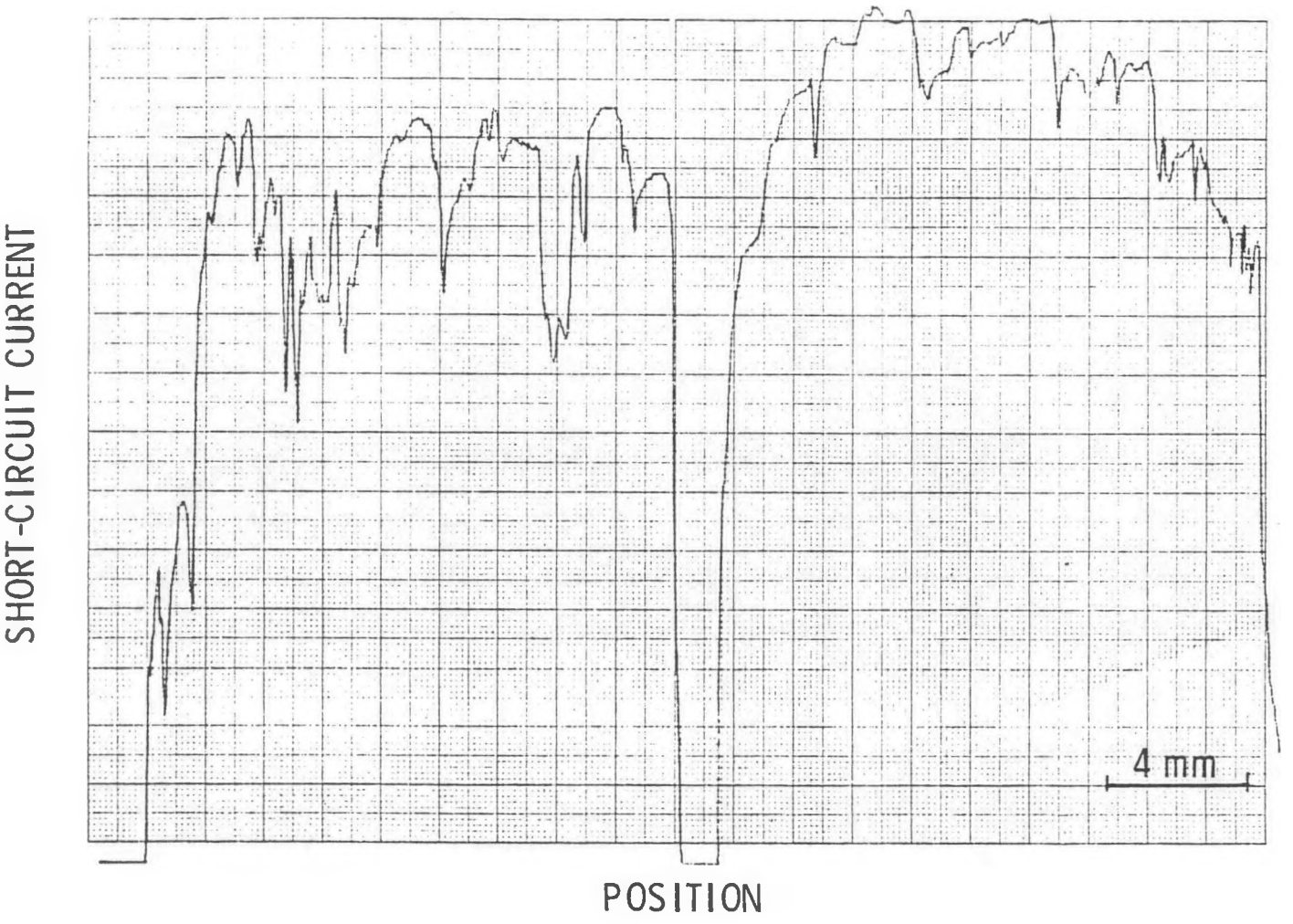

Fig. 31 Photoresponse scan across the width of a polycrystalline silicon solar cell using 8251 Å radiation.

area cells is usually 7.5 to 8.5% at room temperature. The variation of open-circuit voltage, short-circuit current density, fill factor and AM1 efficiency of a solar cell is shown in Figure 32. The open-circuit voltage, fill factor, and conversion efficiency all decreased with increasing temperature while the short-circuit current density increased with increasing temperature, as expected. The open-circuit voltage decreased from 730 mV at $-40^{\circ}C$ to 350 mV at $103^{\circ}C$, and this variation is essentially linear with a slope of -2.8 mV/$^{\circ}C$, as compared with about -2 mV/$^{\circ}C$ for single crystalline silicon solar cells. [28] The short-circuit current density also varies linearly with temperature at a slope of about 0.034 mA/cm^2$^{\circ}C$, very similar to the temperature coefficient of single crystalline silicon solar cells.[28] The fill factor of the solar cell was found to decrease from 70% at $-40^{\circ}C$ to 53% at $103^{\circ}C$. Its AM1 efficiency decreased from 9.5% at $-40^{\circ}C$ to 4.3% at $103^{\circ}C$, and the rate of decrease is about 0.036%/$^{\circ}C$. The characteristics of the solar cell remain unchanged after temperature cycling between $-40^{\circ}C$ and $100^{\circ}C$. These results indicate that the performance of polycrystalline silicon solar cells on graphite compares favorably with that of single crystalline silicon solar cells with regard to the dependence of device parameters on temperature. At temperatures of $-150^{\circ}C$ or below, solar cells fractured due presumably to dissimilar thermal expansion coefficients of the silicon and the RTV-615 encapsulant. Cell destruction occurred within the polycrystalline silicon rather than at the graphite-silicon interface, indicating the strong bonding between graphite and silicon.

Several solar cells were heated at $115^{\circ}C$ for up to 160 hours, and no change in characteristics was observed. They were also subjected to temperature cycling between $-40^{\circ}C$ and $+100^{\circ}C$; the heating and cooling

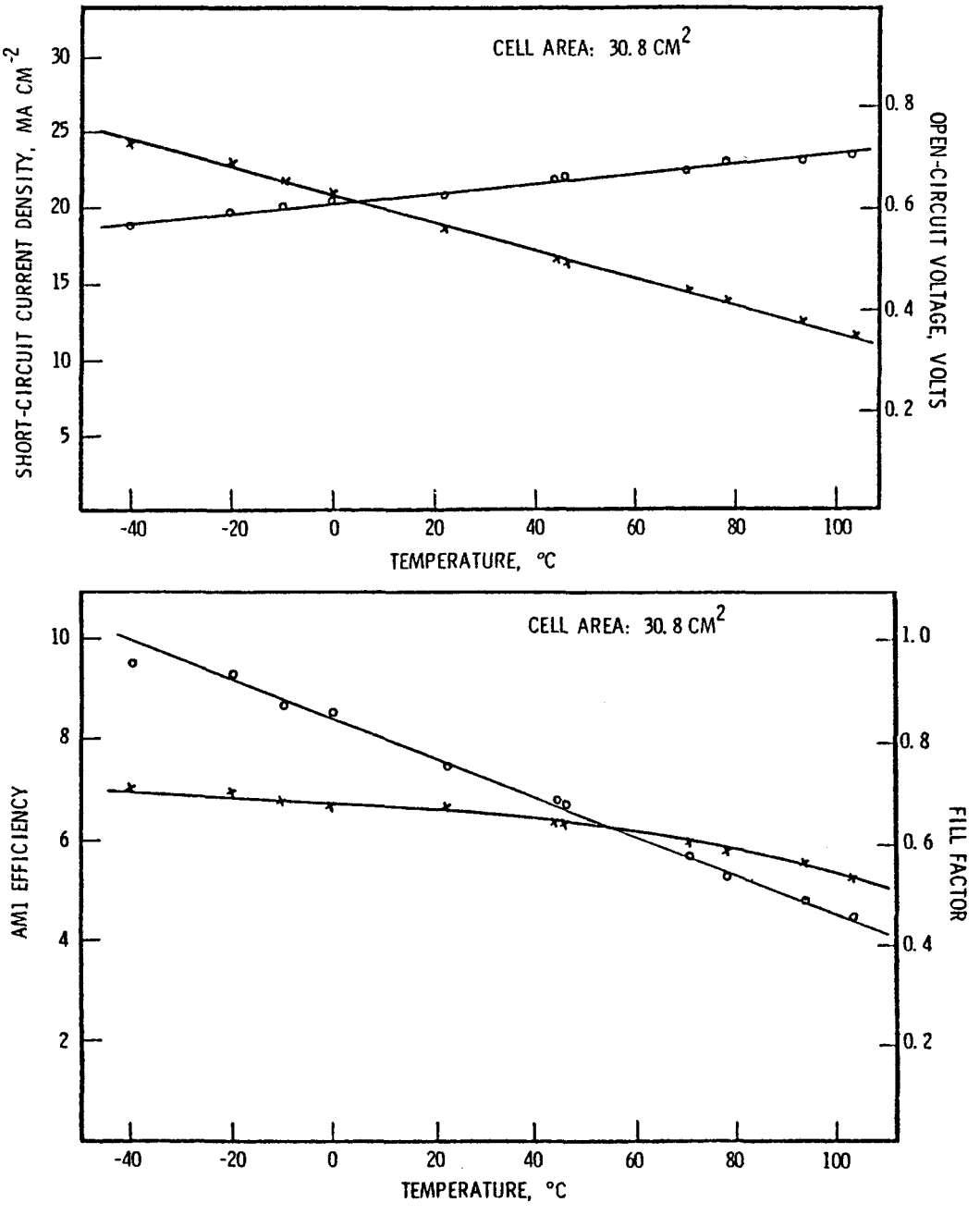

Fig. 32 Characteristics of a large area thin film polycrystalline silicon solar cell as a function of temperature.

were carried out at a rate of about 7^{o}/min, and the cell was maintained at the desired temperature for one hour. The results of a typical test are shown in Table V, where no degradation was observed after 20 cycles.

Table V Effects of temperature cycling on characteristics of a solar cell.

No. of Cycles	V_{oc}(V)	I_{sc}(mA)	FF
0	0.54	406	0.65
9	0.545	410	0.60
15	0.545	410	0.62
20	0.545	410	0.65

To determine their stability under high humidity conditions, thin film silicon solar cells were placed in a reflux apparatus containing boiling deionized water. The humidity was then effectively 100% with condensation of water occuring on solar cells and condenser walls and draining back into the reflux reservoir. The results of a typical test are shown in Table VI; some apparent variations in cell parameters may be associated with water absorption and desorption by RTV. The characteristics were generally measured several hours after the cells were removed from the reflux apparatus.

Table VI Effects of humidity on characteristics of a solar cell.

Time(h)	V_{oc}(V)	I_{sc}(mA)	FF
0	0.544	414	0.63
6	0.55	419	0.60
12	0.543	410	0.64
16	0.543	414	0.63

A solar cell was illuminated under a power density of 1.2 W/cm^2 at 150°C with a 0.2 ohm load for 150 hours. Some degradation in cell characteristics was observed due presumably to the deterioration of the grid contact. The open-circuit voltage, short-circuit current, and fill factor were 0.562V, 620 mA, and 71% respectively before testing, and were 0.55V, 605 mA, and 62%, respectively, after testing.

In summary, the temperature coefficients of parameters of thin film solar cells compare favorably with those of single crystalline silicon solar cells. The thin film solar cells are stable under thermal stress and high humidity conditions indicating that they are promising for terrestrial applications.

VI. 8. Preliminary Cost Analysis

The thin film polycrystalline silicon solar cell developed in this program consists of four steps :

(1) The purification of metallurgical silicon by acid-extraction and phosphorus pentoxide treatment.

(2) The preparation of metallurgical silicon substrates by the recrystallization of the melt on graphite.

(3) The deposition of the active region of the solar cell, a p-n junction structure, on metallurgical silicon substrates by the thermal reductic of trichlorosilane.

(4) The application of grid contacts and antireflection coatings.

The advantages of the above approach are:

(1) Lower-cost metallurgical silicon and graphite are substituted for high-cost single crystal silicon.

(2) Costly processing operations, such as slicing, surface preparation, diffusion, and back ohmic contact making, are eliminated.

(3) Chemical vapor-deposited silicon has better structural perfection than diffused material.

(4) Rectangular geometries permit high cell packing factors.

(5) Any technical innovation which lowers the cost of operations such as anti-reflective coating applications, interconnection, array packaging, etc., will apply equally well to thin film cells.

(6) The development of low-cost metallurgical silicon or solar-grade silicon will also benefit this technology.

A preliminary cost projection for the manufacture of thin film silicon solar cell structures has been made; the costs of front metal contacts, AR coating, interconnection, encapsulation, assembly, and testing are essentially the same as those for other types of silicon solar cells and are not included here. The materials required are (1) graphite and partially purified metallurgical silicon for the preparation of substrates, and (2) trichlorosilane, hydrogen, and doping gases for the deposition of the active region. Their costs per square meter are as follows:

(1) 2-3mm of POCO Graphite Sheet	$ 5.00/m^2
(A new technology under development at POCO Graphite is expected to provide materials in this price range)	
(2) 1mm of partially purified metallurgical silicon at $1.80/kg	4.10/m^2
(3) Trichlorosilane at $1.40/kg and a conversion efficiency of 40%	1.05/m^2
(4) Hydrogen at 0.02/ft^3 and a $H_2/SiHCl_3$ molar ratio of 30	0.25/m^2
(5) Doping gases	0.10/m^2
TOTAL COST	$10.50/$m^2$

As a comparison, the cost of polycrystalline silicon required to produce

silicon sheets of 250 μm thickness is $12.80/m^2, assuming that polycrystalline silicon at a cost of $10/kg is converted to sheet directly. The cost of polycrystalline silicon would be increased to about $25/m^2 if the ingot technology is used.

The processing costs depend strongly on the capacity of the manufacturing equipment. On a pilot scale, the recrystallization equipment could produce 1 m^2 of solar cell per run at a rate of at least 5 runs per shift per day. The chemical vapor deposition of the active region is simpler in operation than the recrystallization process and the conventional silicon epitaxial growth process. The deposition equipment could have twice the capacity of the recrystallizer, i.e., 2 m^2 of solar cell per run at a rate of at least 5 runs per shift per day. Assuming that two operators at an hourly rate of $5 can operate three pieces of equipment, two for recrystallization and one for deposition, the labor cost for recrystallization and deposition is $8/$m^2$. The total material and labor cost is therefore $18.5/$m^2$. By adapting automated processing, there should be room for significant reduction in materials and labor costs.

Assuming a 10% conversion efficiency, the cost per watt of solar cell structure is about 19¢/watt, to which the cost of contacts still has to be added. This compares favorably with the projected costs of silicon, sheet fabrication, back diffusion, junction formation, and back contacting in the low-cost solar array project, $0.253/Wp.

VII. Grain Boundaries in Polycrystalline Silicon Solar Cells

Silicon is an indirect gap material with a very gradual absorption edge, and relative long diffusion length is required to achieve reasonable conversion efficiencies in solar cells. Thus, grain boundaries in silicon play a more important role in solar cell performance than those in direct gap materials. The recombination of photogenerated carriers at grain boundaries in silicon solar cells has been well demonstrated. The reduced minority carrier diffusion length and photoresponse at grain boundaries have been illustrated in Figs. 26 and 31, respectively. Figure 33 shows the secondary electron emission and EBIC photographs of the same area of a thin film polycrystalline silicon solar cell, where the effects of grain boundaries on the collection of beam-induced current are apparent.

The angle between grains also affects the carrier recombination at the boundaries. The carrier recombination at a large angle grain boundary is more pronounced than that at a smaller angle boundary. An example is shown in Fig. 34. The upper photographs are the EBIC micrographs of two specimens containing grain boundaries at angles of approximately 5^{o} and 20^{o}, respectively. The lower photographs show the electron beam induced current profiles at 30 keV scanned along the lines indicated in the upper photographs, and the scans were made at the same signal level for ease of comparison. It is apparent that the decrease in collection efficiency at the 20^{o} angle boundary is more pronounced than that at the 5^{o} degree angle boundary.

To minimize the carrier recombinations at grain boundaries, the electric fields near the boundaries must be modified. This can be achieved by encasing the grain in a charge-collection boundary as shown schematically in Fig. 35. The base region of the solar cell is assumed to be of p-type conductivity,

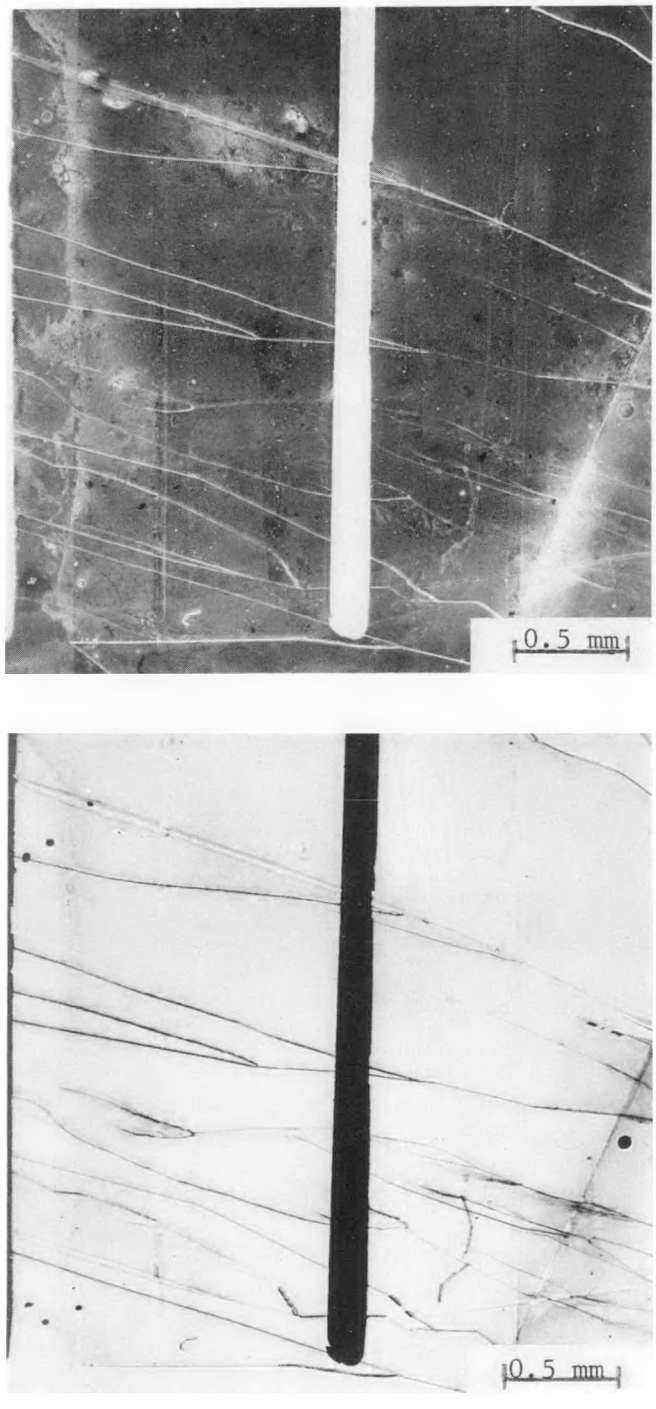

Fig. 33 The secondary electron emission (upper) and EBIC mode (lower) photographs of the same area of a polycrystalline silicon solar cell.

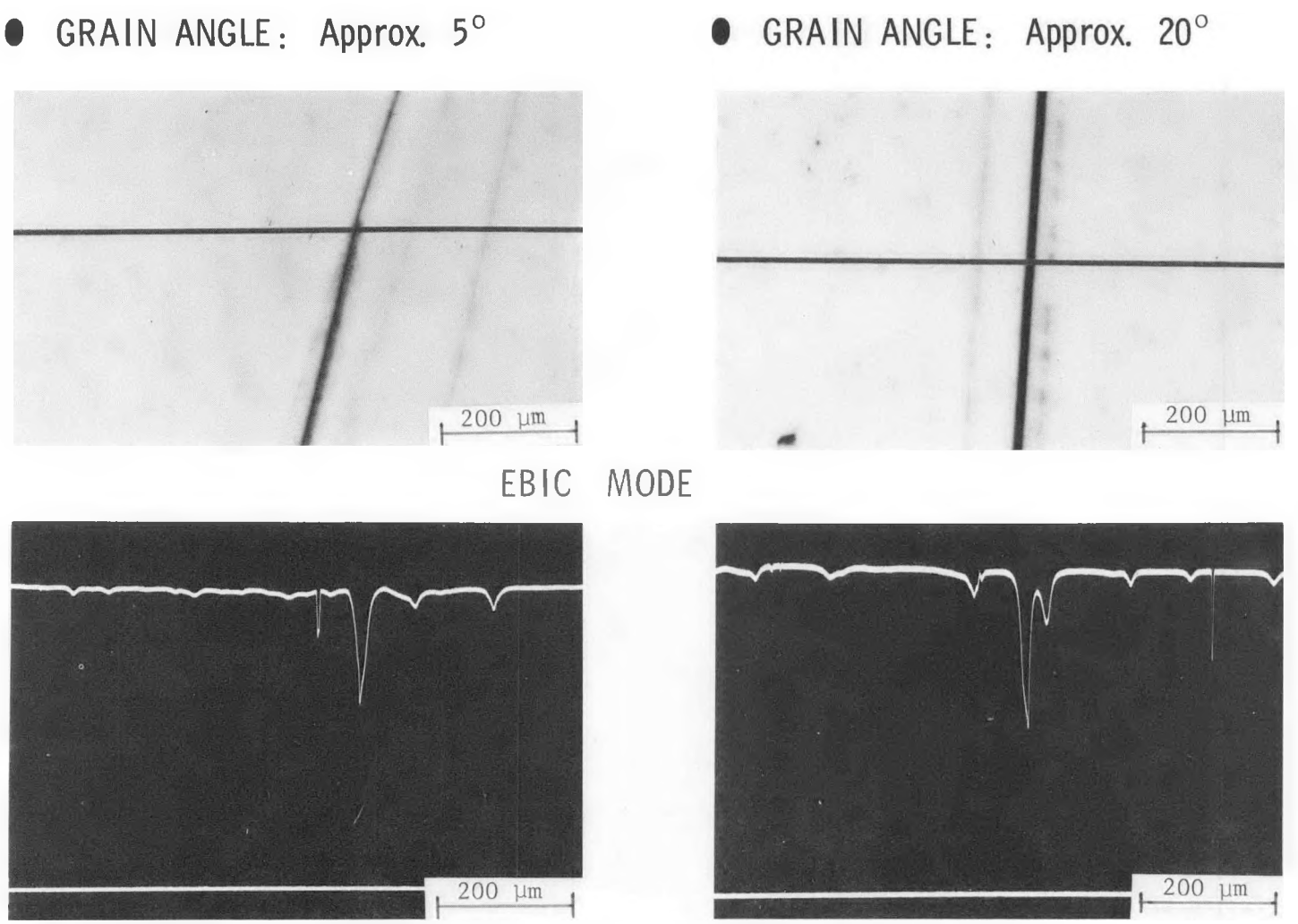

Fig. 34 EBIC photographs and associated electron beam induced current profiles in two specimens containing grain boundaries at different angles.

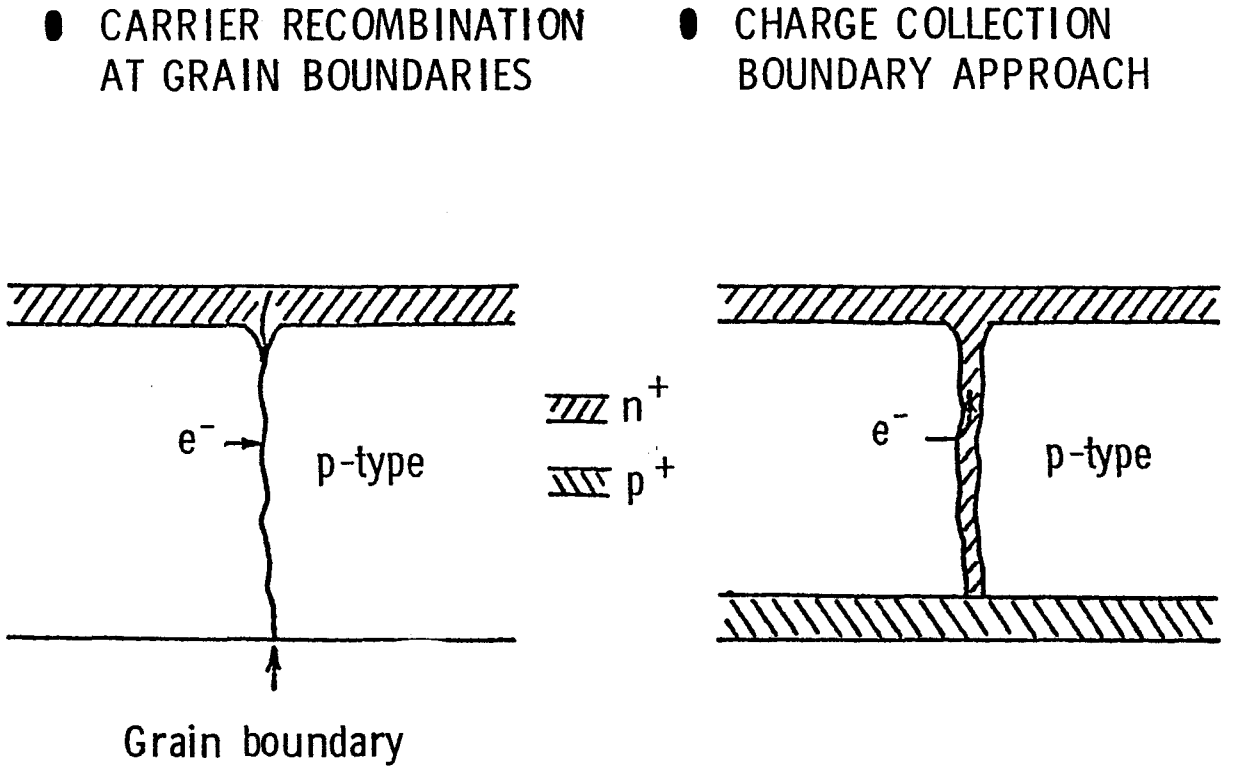

Fig. 35 The charge collection boundary approach for the reduction of grain boundary effects.

and the surface n-region is heavily doped. Any hole-electron pairs generated closer to the grain boundary than the junction will, on the average, be lost by recombination at the grain boundary. However, if the grain boundary is doped preferentially to form a p-n junction, which is electrically connected to the surface junction, electrons reaching the grain boundary are collected by the junction and n-type region. This situation is similar to a vertical junction cell as the grain structure is columnar. The charge collection boundary can be produced by utilizing the difference in the activation energies of bulk diffusion and grain boundary diffusion, and proper heat treatment of the vapor-deposited solar cell could yield such a structure.

Many solar cell structures have been heated at 800° - 950°C in a hydrogen atmosphere for various durations before the contacting process. Invariably, solar cell structures subjected to heat treatment showed higher conversion efficiencies than those without heat treatment. Both photoresponse scan and EBIC techniques were used for the evaluation of the effects of heat treatment and the optimization of heat treatment conditions. These experiments were partially successful; improvements in photoresponse and current collection at grain boundaries were observed only in some specimens as illustrated below. Figure 36 shows the photoresponse profiles at 8251 Å over the surface of a solar cell before and after heat treatment at 850°C. The integrated response is expressed in terms of "loss factor" defined as

$$1 - \frac{\text{area under scan}}{\text{area of rectangle from maximum signal}}$$

In the solar cell under consideration, the loss factor was reduced from 16% to 10.4%. However, the loss factor in the same region showed no appreciable change when 8860 Å radiation was used (Fig. 37). This is due presumably to the small absorption coefficient in silicon, and a significant fraction of radiation is

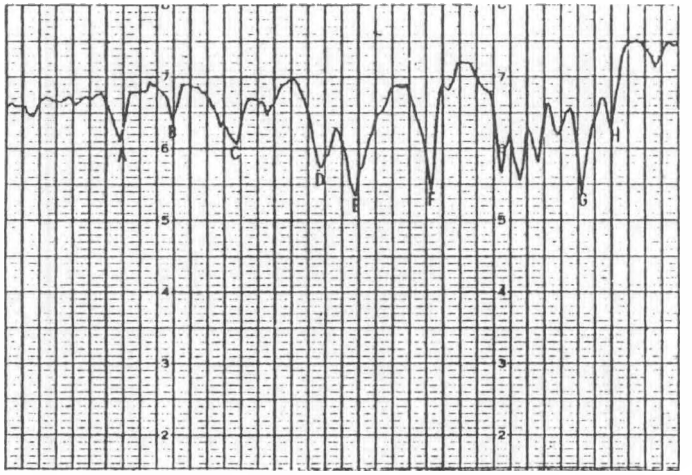

BEFORE HEAT TREATMENT

LOSS FACTOR = 16%

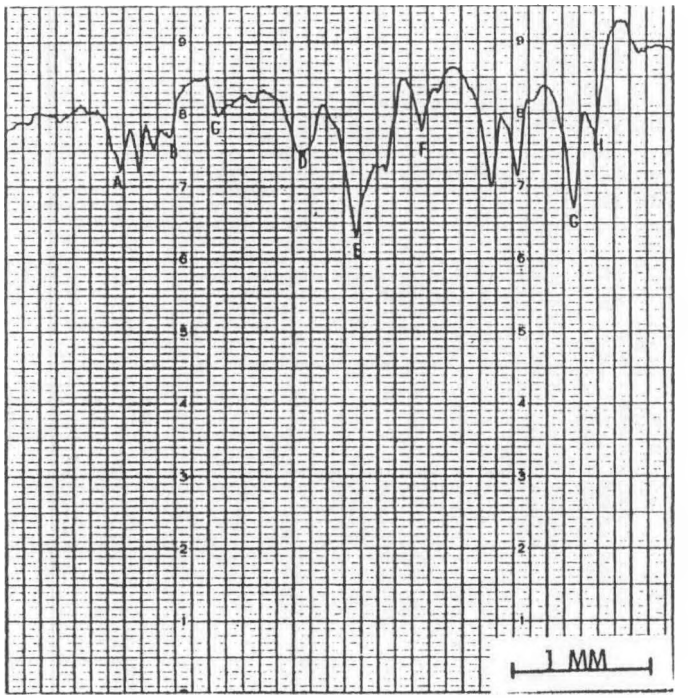

AFTER HEAT TREATMENT AT 850°C

LOSS FACTOR = 10.4%

$$\text{LOSS FACTOR} = 1 - \frac{\text{Area under scan}}{\text{Area of rectangle from maximum signal}}$$

Fig. 36 Photoresponse profiles at 8251 Å over the surface of a solar cell before and after heat treatment at 850°C.

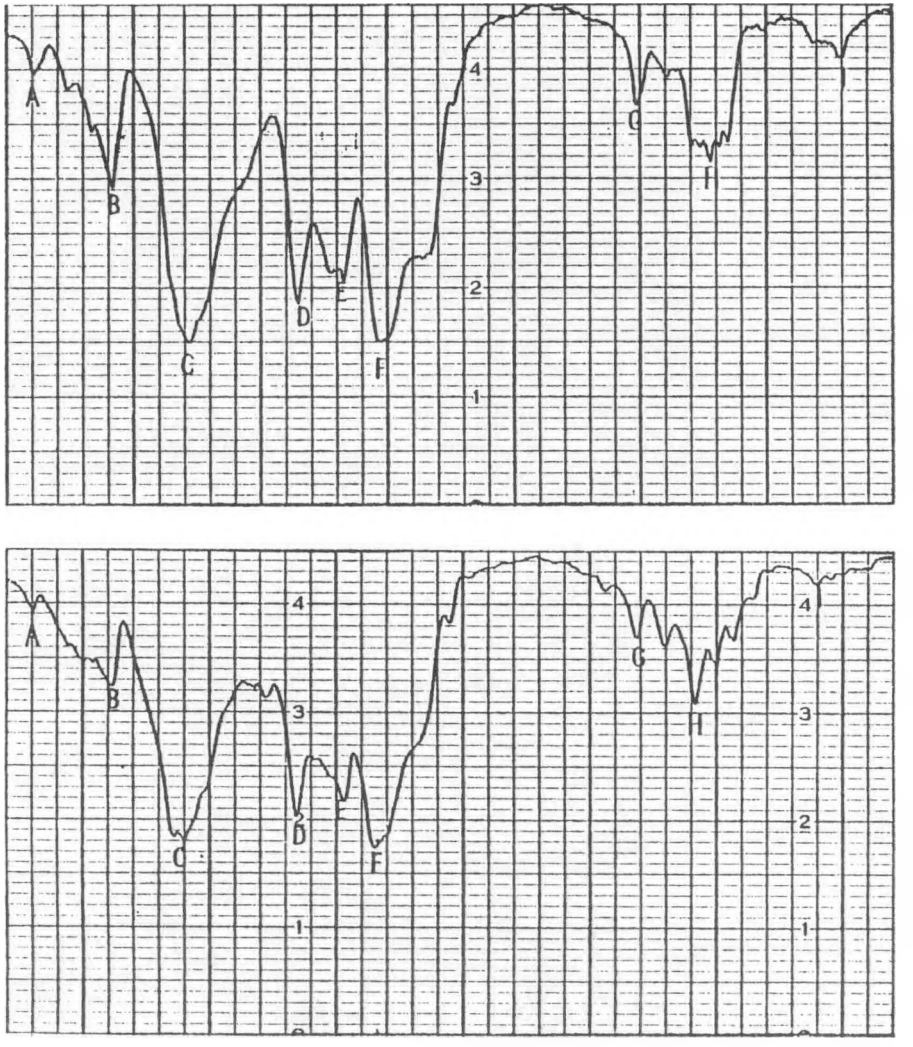

BEFORE HEAT TREATMENT

LOSS FACTOR = 18.5%

AFTER HEAT TREATMENT AT 850°C

LOSS FACTOR = 17.1%

Figure 37 Photoresponse profiles at 8860 Å over the surface of a solar cell before and after heat treatment at 850°C.

absorbed in the substrate. Figure 38 shows the EBIC photograph (10 keV electron energy) of one region of a solar cell after heat treatment at 850°C and the associated line scan illustrating the enhanced current collection at grain boundaries. However, such enhancements in photo-response and current collection are not always observed. This may be due to the precipitation of metallic impurities at structural defects masking the charge collection effects of vertical p-n junctions.

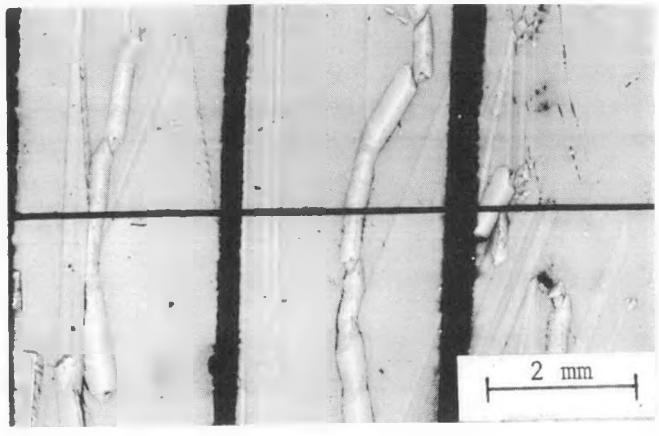

(A)

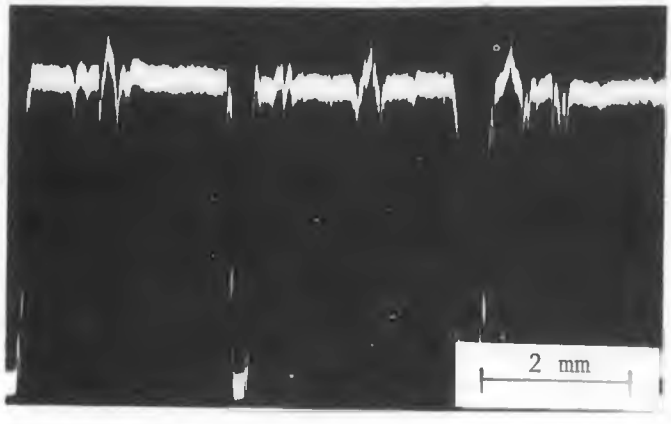

(B)

Fig. 38 EBIC photograph (A) and the associated induced current profile (B) in a thin film silicon solar cell.

VIII. References

(1) P. H. Fang, L. Ephrath, and W. B. Nowak, "Polycrystalline Silicon Films on Aluminum Sheets for Solar Cell Application," Appl. Phys. Letters, 25, 583 (1974).

(2) T. L. Chu, H. C. Mollenkopf, and Shirley S. Chu, "Polycrystalline Silicon on Coated Steel Substrates," J. Electrochem. Soc., 122, 1681 (1975).

(3) T. L. Chu, H. C. Mollenkopf, and Shirley S. Chu, "Deposition and Properties of Silicon on Graphite Substrates," J. Electrochem. Soc., 123, 106 (1976).

(4) C. Feldman, H. K. Charles, Jr., F. G. Satkiewicz, and N. A. Blum, "Vacuum-Deposited Polycrystalline Silicon Solar Cells," in Conference Record, 12th IEEE Photovoltaic Specialists Conference, P. 100, Baton Rouge, Louisiana, November, 1976.

(5) E. Enk and J. Nickel, "Purification of Molten Silicon," German Patent 1,098,931, Feb. 9, 1961.

(6) W. Voos, "Production of Pure Silicon," U. S. Patent 2,972,521, Feb. 21, 1961.

(7) C. J. Brockbank, "Process for Purifying Silicon," U. S. Patent 1,180,968, April 25, 1916.

(8) F. A. Trumbore, "Solid Solubilities of Impurity Elements in Germanium and Silicon," Bell Syst. Tech. J., 39 , 205 (1960).

(9) L. P. Hunt, V. D. Dosaj, J. R. McCormick, and L. D. Crossman, "Production of Solar-Grade Silicon from Purified Metallurgical Silicon," Record of the 12th IEEE Photovoltaic Specialists Conference, Nov. 1976, p. 125.

(10) L. G. Saywell and B. B. Cunningham, "Determination of Iron," Ind. Eng. Chem., Anal. Ed., 9, 67 (1937).

(11) F. C. Hummell and H. H. Willard, "Determination of Iron in Biological Materials," ibid., 10, 13 (1938).

(12) W. C. Dash, "Copper Precipitation on Dislocations in Silicon," J. Appl. Phys., 27, 1193 (1956).

(13) A. G. Tweet, "Precipitation in Semiconductors," J. Appl. Phys., 30, 1244 (1959).

(14) A. Goetzberger and W. Schockley, "Metal Precipitates in Silicon p-n Junctions," J. Appl. Phys., 31, 1821 (1960).

(15) S. W. Ing, Jr., R. E. Morrison, L. L. Alt, and R. W. Aldrich, "Gettering of Metallic Impurities from Planar Silicon Diodes," J. Electrochem. Soc., 110,533 (1963).

(16) J. L. Lambert & M. Reese, "The Gettering of Gold and Copper from Silicon," Solid State Electronics, 11, 1055 (1968).

(17) S. P. Murarka, "A Study of the Phosphorus Gettering of Gold in Silicon by Use of Neutron Activation Analysis," J. Electrochem. Soc., 123, 765 (1976).

(18) L. L. Kazmerski, Solar Energy Research Institute, private communication.

(19) R. J. Stirn, "Junction Characteristics of Silicon Solar Cells," Conference Record of the 9th IEEE Photovoltaic Specialists Conference, May 1972, p. 72.

(20) E. O. Johnson, "Large-Signal Surface Photovoltage Studies with Germanium," Phys. Rev., 111,153 (1958).

(21) A. M. Goodman, "A Method for the Measurement of Short Minority Carrier Diffusion Lengths in Semiconductors," J. Appl. Phys., 32, 2550 (1961).

(22) W. E. Phillips, "Interpretation of Steady-State Surface Photovoltage Measurements in Epitaxial Semiconductor Layers," Solid State Electronics, 15, 1097 (1972).

(23) ASTM F391-78, "Standard Test Method for Minority Carrier Diffusion Length in Silicon by Measurement of Steady-State Surface Photovoltage, "1978 Annual Book of ASTM Standards, ASTM, Philadelphia, Pa., 1978, p. 776.

(24) E. Y. Wang, C. R. Baraona, and H. W. Brandhorst, Jr., "Surface Photovoltage Method Extended to Silicon Solar Cell Junction," J. Electrochem. Soc., 121, 973 (1974).

(25) T. S. Moss, G. J. Barrell, and B. Ellis, Semiconductor Opto-Electronics, John Wiley and Sons, New York, N. Y. 1973, p. 182.

(26) W. R. Runyan, "A Study of the Absorption Coefficient of Silicon in the Wavelength Region between 0.5 and 1.1 μ," Southern Meth. Univ. Report 83-13, 1967 (NASA CR 93154).

(27) D. E. Sawyer, "A Technique for Using an Optical Scanner to Reveal Solar Cell Defects." Conference Record of the 13th IEEE Photovoltaic Specialists Conference, June 1978, p. 1249.

(28) J. D. Sandstrom, "A Method for Predicting Solar Cell Current-Voltage Characteristics as a Function of Incident Solar Intensity and Cell Temperature," Conference Record of the 6th IEEE Photovoltaic Specialists Conference, March, 1967, p. 199.

IX. Conclusions and Recommendations for Future Work

IX.1. Conclusions

1. A combination of the chemical treatment of melt and unidirectional solidification can be used to remove a major portion or metallic impurities in silicon. The use of acid extraction and phosphorus pentoxide treatment, though less efficient, is the most economical technique for the partial purification of silicon, and the resulting material is suitable as a substrate for the deposition of the active region of solar cells.
2. The microstructure of metallurgical silicon recrystallized on graphite depends strongly on the rate of solidification; planar surfaces are obtained at low rates and dendritic surfaces are obtained at high rates.
3. The thermal reduction of trichlorosilane has been used to deposit epitaxial silicon films of controlled thickness and dopant distribution on metallurgical silicon substrates. At carrier concentrations of 10^{17} cm^{-3} or lower, the potential barrier across a grain boundary in epitaxial silicon films becomes appreciable.
4. The grain boundaries in passivated epitaxial mesa diodes do not have appreciable effects on the dark current-voltage characteristics, and the recombination process at grain boundaries can be included in those in the space charge region without introducing a third exponential term.
5. The extension of the surface photovoltage technique to the measurement of short-circuit current is a simple and reproducible technique for the measurement of minority carrier diffusion length in the base region of solar cells.
6. Grain boundaries in thin film silicon solar cells reduce (1) the local diffusion length of minority carriers, (2) the photoresponse, and (3) the collection of beam-induced current. The effects of grain boundaries can be minimized by heat treatment.

7. The temperature dependence of characteristics of thin film polycrystalline silicon solar cells compare favorably with that of single crystalline cells. Thin film cells are stable under conditions encountered in terrestrial applications.
8. Thin film polycrystalline silicon solar cells of 9 cm^2 area with an AM1 efficiency of about 9.75% have been produced.

IX. 2. Recommendations for Future Work

1. Scaling-up of the technology developed in this program to determine its potential for manufacturing.
2. Development of alternate technology for the preparation of metallurgical silicon substrates.
3. Improvement of chemical and structural perfection of purified metallurgical silicon substrates so that diffusion instead of CVD may be used for junction formation.

X. Publications and Research Contributors

X. 1. Oral Presentations

1. "Large Area High Efficiency Polycrystalline Silicon Solar Cells," presented at the 150th National Meeting of the Electrochemical Society, Las Vegas, Nevada, October, 1976. Electrochem. Soc. Extended Abstracts, 76-2,899-900 (1976).

2. "Silicon Solar Cells on Metallurgical Silicon Substrates," presented at the 12th IEEE Photovoltaic Specialists Conference, Baton Rouge, Louisiana. November, 1976. Conference Record, 74-75.

3. "A Novel Method for the Measurement of Diffusion Lengths in Solar Cells," Presented at the 1976 International Electron Device Meeting, Washington, D. C. December, 1976. Technical Digest, 478-490.

4. "Polycrystalline Silicon P-N Junctions," presented at the 151st National Meeting of the Electrochemical Society, Philadelphia, Pa., May 8-13, 1977. Electrochem. Soc. Extended Abstract, 77-1, 270-271 (1977).

5. "Diffusion Length in Single Crystalline Silicon Slices by Surface Photovoltage Measurements," presented at the 19th Electronic Materials Conference, Ithaca, New York, June 1977.

6. "Polycrystalline Semiconductor Films for Solar Cells," presented at the symposium on Preparation, Properties, and Applications of Crystals and Films, National Meeting of the American Chemical Society, Chicago, Ill. August 28-September 2, 1977.

7. "Polycrystalline Silicon Solar Cells," presented at the 152nd National Meeting of the Electrochemical Society, Atlanta, Georgia, October, 1977. Extended Abstracts, 77-2, 800 (1977).

8. "Stability of Thin Film Polycrystalline Silicon Solar Cells," presented at the Stability of Solar Cells and Materials Workshop, Gaithersburg, Maryland, May 1-3, 1978.

9. "Diffusion Length Inhomogeneities in Single Crystalline Silicon Solar Cells," presented at the 13th IEEE Photovoltaic Specialists Conference, June 5-8, 1978, Washington, D. C. Conference Record, 95-99.

10. "Polycrystalline Silicon Solar Cells," presented at the 13th IEEE Photovoltaic Specialists Conference, June 5-8, 1978, Washington, D. C. Conference Record, 1106-1110.

11. "Thin Film Silicon Solar Cells," presented at the Subpanel Meeting on Thin Film Solar Cells, American Physical Society Study on Solar Photovoltaic Energy Conversion, June 9, 1978, Washington, D. C.

12. "Thin Film Polycrystalline Silicon Solar Cells," presented at the Distinguished Lecture Series on Solar Cells, University of Cincinnati, July 17, 1978, Cincinnati, Ohio.

13. "Thin-Film Polycrystalline Silicon Solar Cells," presented at the MIT Lincoln Laboratory Solid State Seminar, September 12, 1978, Lexington, Mass.

14. "Stability of Thin Film Polycrystalline Silicon Solar Cells," presented at the 154th National Meeting of the Electrochemical Society, Pittsburgh, Pa., October, 1978. Extended Abstracts, 78-2, 795 (1978).

15. "Effective Diffusion Length in Polycrystalline Thin Films," presented at the Photovoltaic Material and Device Measurements Workshop, June 11-13, 1979, Arlington, Va.

X. 2. Scientific Papers

1. "Silicon Solar Cells on Unidirectionally Solidified Metallurgical Silicon," IEEE Trans. Electron Devices, ED-24, 442 (1977).

2. "Diffusion Lengths in Solar Cells from Short-Circuit Current Measurements," Appl. Phys. Letters, 30, 425 (1977).

3. "Silicon Films on Foreign Substrates for Solar Cells," J. Crystal Growth, 39, 45 (1977).

4. "Silicon Solar Cells on Zone-Melted Silicon/Graphite Substrates," J. Appl. Phys., 48, 3576 (1977).

5. "Minority Carrier Diffusion Length in Silicon Slices and Shallow Junction Devices," J. Electronic Materials, 7, 173 (1978).

6. "A Comparison of Carrier Lifetime Measurements by Photoconductive Decay and Surface Photovoltage Methods," J. Appl. Phys., 49, 2996 (1978).

7. "Solar Cells from Zone-Refined Metallurgical Silicon," J. Electrochem. Soc., 125, 595 (1978).

8. "Purification and Characterization of Metallurgical Silicon," J. Electrochem. Soc., 125, 661 (1978).

9. "Polycrystalline Silicon P-N Junctions," Solid State Electronics, 21, 781 (1978).

10. "High Efficiency Thin Film Polycrystalline Silicon Solar Cells," J. Appl. Phys., 50, 919 (1979).

11. "Large Grain Silicon Films on Metallurgical Silicon Substrates for Photovoltaic Applications," Solar Energy Materials, in press.

X. 3. Patent

"Process for Utilizing Low-Cost Graphite Substrates for Polycrystalline Solar Cells," U. S. Patent 4,077,818. March 7, 1978.

X. 4. Research Contributors

Dr. Ting L. Chu, Professor and Principal Investigator

Dr. Shirley S. Chu, Associate Professor

Dr. Everett D. Stokes, Research Assistant Professor

Dr. Gerard A. van der Leeden, Research Associate

Dr. Hyouk I. Yoo, Research Associate

Dr. John M. Herman III, Consultant

Dr. K. H. Hong, Consultant

Mr. Roshdy Abderrassoul, Graduate Student

Mr. Mike Hensley, Graduate Student

Mr. Chin J. Lin, Graduate Student

Mr. Ching L. Lin, Graduate Student

Mr. Ian C. Harris, Technician

☆U.S. GOVERNMENT PRINTING OFFICE: 1980-640-258/2323